Cosmogenic nuclide exposure age scatter in McMurdo Sound, Antarctica records Pleistocene glacial history and processes

Andrew J. Christ[1], Paul R. Bierman[1,2], Jennifer L. Lamp[3], Joerg M. Schaefer[3], Gisela Winckler[3]

[1]Gund Institute for Environment, University of Vermont, Burlington, VT, 05405, USA

[2]Rubenstein School of the Environment and Natural Resources, University of Vermont, Burlington, VT, 05405, USA

[3]Lamont Doherty Earth Observatory, Columbia University, Palisades, NY 10964, USA

Correspondence to: Andrew Christ (Andrew.Christ@uvm.edu)

Abstract. The preservation of cosmogenic nuclides that accumulated during periods of prior exposure but were not subsequently removed by erosion or radioactive decay, complicates interpretation of exposure, erosion, and burial ages used for a variety of geomorphological applications. In glacial settings, cold-based, non-erosive glacier ice may fail to remove inventories of inherited nuclides in glacially transported material. As a result, individual exposure ages can vary widely across a single landform (e.g., moraine) and exceed the expected or true depositional age. The surface processes that contribute to inheritance remain poorly understood, thus limiting interpretations of cosmogenic nuclide datasets in glacial environments. Here, we present a compilation of new and previously published exposure ages of multiple lithologies in local Last Glacial Maximum (LGM) and older Pleistocene glacial sediments in the McMurdo Sound region of Antarctica. Unlike most Antarctic exposure chronologies, we are able to compare exposure ages of local LGM sediments directly against an independent radiocarbon chronology of fossil algae from the same sedimentary unit that brackets the age of the local LGM between 12.3 and 19.6 ka. Cosmogenic exposure ages vary by lithology, suggesting that bedrock source and surface processes prior to, during, and after glacial entrainment explain scatter. ^{10}Be exposure ages of quartz in granite, sourced from the base of the stratigraphic section in the Transantarctic Mountains, are scattered but young, suggesting that clasts entrained by sub-glacial plucking can generate reasonable apparent exposure ages. ^{3}He exposure ages of pyroxene in Ferrar Dolerite, which crops out above outlet glaciers in the Transantarctic Mountains, are older, which suggests that clasts initially exposed on cliff faces and glacially entrained by rock fall carry inherited nuclides. ^{3}He exposure ages of olivine in basalt from local volcanic bedrock in the McMurdo Sound region contain many excessively old ages, but also have a bimodal distribution with peak probabilities that slightly pre-date and post-date the local LGM; this suggests that glacial clasts from local bedrock record local landscape exposure. With the magnitude and geological processes contributing to age scatter in mind, we examine exposure ages of older glacial sediments deposited by the most extensive ice sheet to inundate McMurdo Sound during the Pleistocene. These results underscore how surface processes operating in the Transantarctic Mountains are expressed in the cosmogenic nuclide inventories held in Antarctic glacial sediments.

1. Introduction: the problem of inherited cosmogenic nuclides

In situ cosmogenic nuclides, which accumulate in near-surface materials during exposure to cosmic radiation, can be measured across a wide range of environments and timescales to quantitatively describe earth surface processes, including quantifying erosion rates (Portenga et al., 2019), dating landforms and exposed bedrock surfaces~~dating landforms and surfaces~~ (Christ et al., 2021a; Wells et al., 1995), reconstructing changes in climate over millions of years (Bierman et al., 2016; Schaefer et al., 2016; Shakun et al., 2018), among many other applications. However, inherited nuclides, those which accumulated in surface material during periods of prior exposure but were not subsequently removed by erosion or through the decay of radioactive nuclides, can produce results that are difficult-to-interpret in surface exposure dating samples. Nuclide inheritance affects nearly all geomorphologic settings – it complicates the interpretation of alluvial fan ages in deserts (Owen et al., 2011), river terrace exposure ages used to determine canyon incision rates (Cook et al., 2009), shore platform erosion rates in coastal settings (Trenhaile, 2018) and glacial chronologies using exposure ages of boulders on moraines or glacially sculpted bedrock (Briner et al., 2014; Corbett et al., 2016; Davis et al., 1999; Young et al., 2016).

Inherited nuclides are prevalent in glacial sediments, from alpine glacier moraines (Briner et al., 2005; Heyman et al., 2011) to glacial erratics transported by polar ice sheets (Brook et al., 1995; Corbett et al., 2019; Hein et al., 2014). Surface exposure ages of glacial deposits are assumed to record the duration of exposure following emplacement and/or glacial retreat, allowing a reconstruction of former ice extent at specific time-slices (Dunai, 2010). In practice, exposure chronologies can yield highly scattered exposure ages that vary widely across a single, contemporaneously deposited landform (i.e., a moraine) and often greatly exceed the expected or true depositional age (Hein et al., 2014; Heyman et al., 2011). Cosmogenic nuclide scatter in glacial environments is likely due to clasts or surfaces that contain nuclides that accumulated during periods of prior exposure but were not subsequently removed by non-erosive, cold-based glacial ice (Briner et al., 2006; Corbett et al., 2019; Koester et al., 2020). Cold-based glaciation occurs where ice thickness and/or basal ice temperatures are insufficient to produce meltwater and basal sliding, both of which facilitate subglacial erosion, and therefore removal of inherited nuclides, in formerly exposed surfaces (Bennett and Glasser, 1996). The basal thermal regime below ice can be highly heterogeneous, resulting in selective erosion of the landscape (Briner et al., 2006; Jamieson et al., 2010; Sugden et al., 2005). Consequently, glacial sediments can be entrained, transported, and deposited by both warm- and cold-based glacial ice, and ultimately produce scattered cosmogenic surface exposure ages (Hein et al., 2014; Heyman et al., 2011).

The problem of inherited nuclides and exposure age scatter is exacerbated in Antarctica, where large polythermal ice sheets, hyper-arid polar desert climate conditions, and extremely low sub-aerial erosion rates have persisted since the Miocene (Lamp et al., 2017; Lewis and Ashworth, 2016; Lewis et al., 2008; Shakun et al., 2018; Sugden and Denton, 2004; Sugden et al., 2006). Glacial sediments in ice-free areas of Antarctica preserve direct geological constraints on former ice sheet configurations from Holocene to Miocene time (Anderson et al., 2020; Balco et al., 2013; Balter-Kennedy et al., 2020; Bromley et al., 2010; Christ and Bierman, 2020; Hall et al., 2015; Jones et al., 2015, 2021; Nichols et al., 2019; Spector et

al., 2017). Cosmogenic nuclides are often the only method available for constraining a numerical chronology of Antarctic glacial deposits. Radiocarbon dating is usually not applicable due to the absence of organic remains and/or because the sedimentary archives are >50 kyr. Low erosion rates have resulted in long-lived exposure of high elevation surfaces that are later covered and/or entrained by cold-based glacier ice that fails to erode and remove inherited nuclides (Balco et al., 2019; Hein et al., 2014; Stone et al., 2003; Sugden et al., 2014). Additionally, debris entrainment via rockfall may introduce nuclide scatter due to differential erosion on cliff-faces (Lamp et al., 2017; Mackay et al., 2014). However, large outlet glaciers and ice streams have also deeply eroded and modified parts of the landscape (Lewis and Ashworth, 2016; Sugden et al., 2005) and transported sediments to terrestrial margins (Stuiver et al., 1981) and onto the continental shelf (Anderson, 1999; Bentley et al., 2014). As a result, many cosmogenic nuclide exposure chronologies from Antarctic terrestrial glacial deposits contain scatter with exposure ages that can span tens to hundreds of thousands of years for individual landforms (Brook et al., 1993; Hein et al., 2014; Joy et al., 2014; Staiger et al., 2006; Swanger et al., 2011).

2. McMurdo Sound: a unique setting to examine cosmogenic nuclide inheritance

Here, we focus on cosmogenic nuclide analyses from ice-free areas surrounding McMurdo Sound, Antarctica (78°S, 165°E), as it is uniquely suited to examine scatter in exposure age datasets from glacial sediments (Fig. 1A). McMurdo Sound hosts one of the largest ice-free areas in Antarctica and contains Pleistocene glacial sediments on volcanic islands and coastal valleys of the Transantarctic Mountains (Christ and Bierman, 2020; Denton and Marchant, 2000; Hall et al., 2015; Hall and Denton, 2000; Jackson et al., 2018; Stuiver et al., 1981) (Fig. 1, 2). The prominence of the Royal Society Range prevents the East Antarctic Ice Sheet (EAIS) from directly discharging into McMurdo Sound. During past glacial periods when southerly EAIS outlet glaciers expanded into the Ross Sea, grounded ice over-rode some or all of the volcanic features in the McMurdo Sound region, impounding the flow of Koettlitz Glacier and other portions of the McMurdo Dry Valleys grounded ice circumvented volcanic features and overflowed into McMurdo Sound from the east (Christ and Bierman, 2020; Denton and Marchant, 2000; Greenwood et al., 2018; Hall et al., 2015; Stuiver et al., 1981) (Fig. 1). These incursions of grounded ice into McMurdo Sound transported and deposited lithologies from the Transantarctic Mountains, including Granite Harbor Intrusives, Ferrar Dolerite, Koettlitz Group metamorphic rocks, Beacon Sandstone, as well as other rocks from the East Antarctic interior (Christ and Bierman, 2020; Denton and Marchant, 2000; Talarico et al., 2012, 2013) (Fig. 1B). Specifically, lithologies present in the AND-1B drill core and erratics in ice-free areas of McMurdo Sound correspond primarily to rocks found along the Mullock and Skelton Glaciers (Talarico et al., 2012, 2013). The diversity of lithologies in glacial sediments in the McMurdo Sound region provides targets for multiple cosmogenic nuclides to calculate exposure ages; yet, previous efforts in the McMurdo Sound region yielded a complex exposure history (Anderson et al., 2017; Brook et al., 1995; Joy et al., 2017).
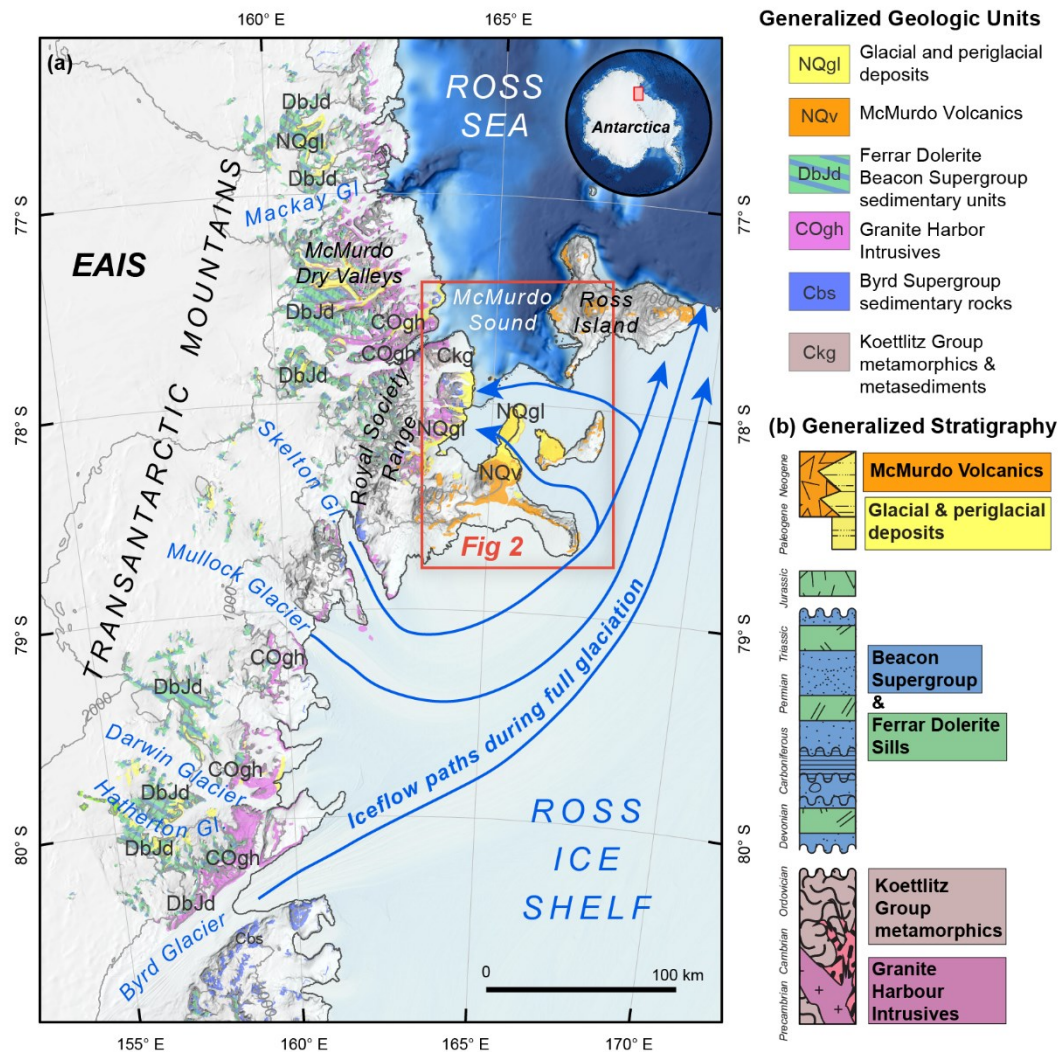
Figure 1: Bedrock geology and generalized stratigraphy of Southern Victoria Land, Antarctica. (a) Regional overview map showing the generalized geologic units of Southern Victoria Land, Antarctica. Blue arrows show the general flow directions of outlet glaciers when expanded into the Ross Sea. Base map uses data from the 2013 International Bathymetric Chart of Southern Ocean (Arndt et al., 2013) and the Reference Elevation Mosaic of Antarctica generated by the Polar Geospatial Center (Howat et al., 2019); generalized bedrock geology adapted from (Grindley and Laird, 1969; Warren, 1969).(b) Generalized stratigraphy of Southern Victoria Land, Antarctica adapted from (Fitzgerald, 2002).

The ice-free islands and peninsulas of McMurdo Sound contains at least two different Pleistocene glacial

sedimentary units (Denton and Marchant, 2000). At lower elevations (<510 m), the local Last Glacial Maximum (LGM) glacial deposit, known locally as Ross Sea drift, is characterized by a high concentration of erratic lithologies and un-weathered clasts that lack iron-staining or ventifaction (Christ and Bierman, 2020; Denton and Marchant, 2000; Hall et al., 2015; Stuiver et al., 1981). Unlike many Antarctic glacial sediments, Ross Sea drift has a robust radiocarbon chronology of fossil algae embedded in moraines and ice-marginal sediments, which indicates that grounded ice maintained its local LGM extent between 12.3 and 19.6 calibrated thousands of years before present (cal. ka) (Christ and Bierman, 2020; Hall et al., 2015; Hall and Denton, 2000; Jackson et al., 2018; Stuiver et al., 1981). A pioneering application of cosmogenic ^{10}Be, ^{26}Al, and ^{3}He in several lithologies from Ross Sea drift produced a highly scattered exposure age dataset ranging from 8 to 106 kyr (Brook et al., 1995). A recent elevation transect of ^{10}Be in quartz (^{10}Be$_{quartz}$) exposure ages of granite boulders along eastern Mount Discovery indicates that ice thinned from its maximum extent no earlier than 14.1 ka to present conditions by 7.6 ka (Anderson et al., 2017). At higher elevations on the ice-free regions of volcanic islands in McMurdo Sound in McMurdo Sound, other glacial sediments remain largely unmapped and undated. These glacial deposits are characterized by a lower concentration of erratic lithologies relative to Ross Sea drift and are presumably older, as indicated by enhanced surface weathering characteristics including chemically-altered surfaces, and ventifacted and cavernously weathered boulders (Denton and Marchant, 2000). Earlier reconnaissance mapping on Mount Discovery indicated these deposits extend up to 770 m elevation (Denton and Marchant, 2000; Stuiver et al., 1981). Other similar higher elevation glacial deposits exist above Ross Sea drift in the Royal Society Range and, while they have not been mapped in detail, have some exposure age constraints that range widely between 104 – 567 kyr (Brook et al., 1995).

There are several advantages to examining exposure ages of glacial deposits the ice-free areas surrounding McMurdo Sound in McMurdo Sound. Exposure ages of clasts from Ross Sea drift can be compared against the independently constrained radiocarbon chronology of fossil algae embedded in moraines and ice-marginal sediments from the same deposit (Fig. 2, 3) (Christ and Bierman, 2020; Hall et al., 2015; Hall and Denton, 2000; Jackson et al., 2018; Stuiver et al., 1981). The diversity of lithologies in glacial sediments in the ice-free areas surrounding McMurdo Sound provides targets for multiple cosmogenic nuclides by which to calculate exposure ages and these different lithologies in glacial sediments from McMurdo Sound can be tied to their bedrock sources in the Transantarctic Mountains (Talarico et al., 2012, 2013). We compiled new and previously published (Anderson et al., 2017; Brook et al., 1995) exposure ages of different lithologies in Ross Sea drift to quantify the magnitude of exposure age scatter and investigate surface processes that contribute to, prevent, or reduce nuclide inheritance in Antarctic terrestrial glacial sediments By examining a compilation of new and previously published exposure ages of different lithologies in Ross Sea drift, we are able to quantify the magnitude of exposure age scatter and investigate surface processes that contribute to, prevent, or reduce nuclide inheritance in Antarctic terrestrial glacial sediments. With the magnitude and pattern of exposure age scatter known, we then examine previously unmapped and undated glacial deposits that delineate the maximum extent of grounded ice on Mount Discovery.
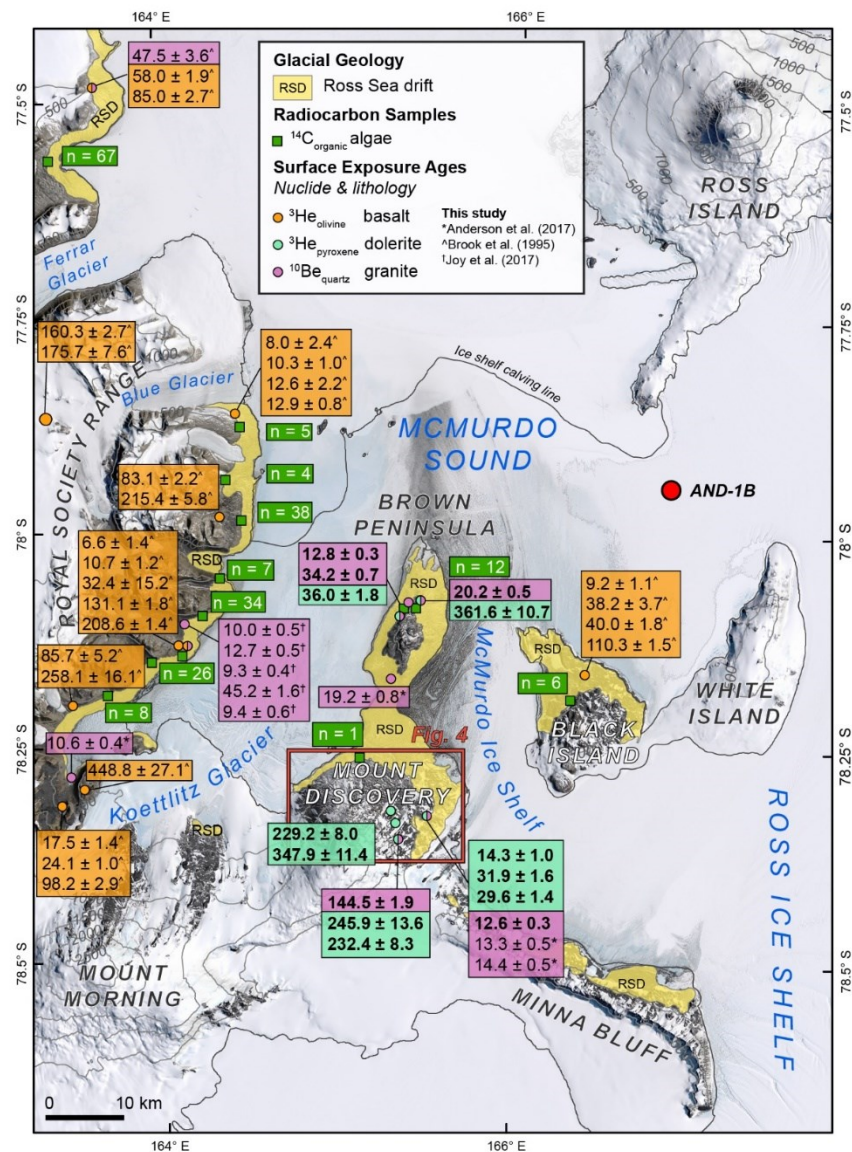
Figure 2: Compiled cosmogenic nuclide exposure ages and radiocarbon sample locations in the McMurdo Sound region. The extent of Ross Sea drift from is shown. The Nnumber of calibrated radiocarbon ages of Ross Sea drift are shown in green boxes (Christ and Bierman, 2020; Hall et al., 2015; Hall and Denton, 2000; Jackson et al., 2018). All exposure ages from this study and previously published data (Anderson et al., 2017; Brook et al., 1995; Joy et al., 2017) were recalculated using the same LSDn scaling scheme (Lifton et al., 2014) and shown here as the exposure age ± 1σ internal uncertainty from previous studies. Extent of Figure 4 shown in white for detailed mapping on Mount Discovery. AND-1B drill core (red circle) shown for reference (McKay et al., 2012). Base map: Landsat Image Mosaic of Antarctica and 500 m contours derived from DEM(s) created by the Polar Geospatial Center from DigitalGlobe, Inc. imagery (Howat et al., 2019).
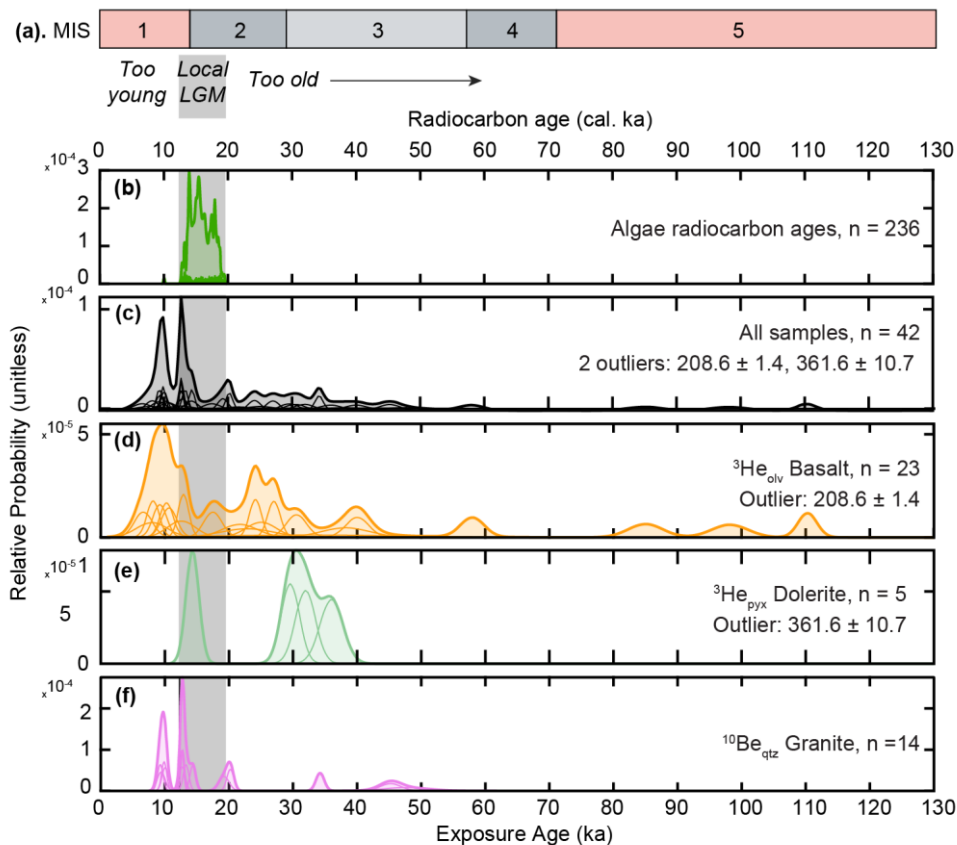
Figure 3: Ross Sea drift age constraints. (a) Marine Isotope Stage (MIS) boundaries and the timing of the local Last Glacial Maximum (LGM) in McMurdo Sound (gray box). Kernel density functions of (b) algae radiocarbon ages, and exposure ages in (c) all samples, (d) $^3He_{olv}$ in basalt (e) $^3He_{pyx}$ in dolerite, and (f) $^{10}Be_{qtz}$ in granite. Thin lines show gaussian distributions of individual sample ages and thick lines show the kernel density functions. Outliers are ages >130 ka.

3. Materials and methods

3.1 Glacial geologic mapping

We built upon the detailed mapping and descriptions of Ross Sea drift on the volcanic islands and peninsulas (Christ and Bierman, 2020; Denton and Marchant, 2000) with new surveys of higher elevation glacial deposits on Mount Discovery (hereafter referred to as the Upper Discovery deposit). The Upper Discovery deposit was mapped at several sites on Mount Discovery at elevations between 450 and 775 m. GPS data points were collected using a handheld Garmin GPS unit (precision <10 m) on moraines and glacial limits. We complemented on-the-ground field mapping with analysis of aerial

photographs, high-resolution (< 1.85 m/pixel) DigitalGlobe, Inc. imagery, and a stereo-photogrammetric digital elevation
model (2 m/pixel) created by the Polar Geospatial Center (Howat et al., 2019).

3.2 Sample collection

Erratic clasts of Granite Harbor Intrusives (granite) and Ferrar Dolerite were collected for cosmogenic ^{10}Be in quartz (^{10}Be$_{qtz}$)
and ^{3}He in pyroxene (^{3}He$_{pyx}$) exposure dating, respectively, from moraine crests and the limits of Ross Sea drift and the
Upper Discovery deposit on the volcanic islands of McMurdo Sound. Clasts that were clearly perched, either on top of other
clasts or on the surface of glacial sediment, were collected over those embedded into sediment to avoid 'young' exposure
ages due to possible exhumation. Samples were collected from local topographic highs (~~i.e.~~i.e., moraine ridge crests) to
avoid local shielding, clast overturning, rotation, exhumation, or downslope movement. The GPS coordinates, topographic
shielding, clast orientation, clast dimensions, weathering characteristics, and geomorphic setting were recorded for each
sample. Samples from larger clasts were collected from the upper 10 cm of rock using a hammer-drill and wedges and shims.
Whole-rock samples of smaller cobble-sized clasts were taken.

3.3 Cosmogenic nuclide analyses

The upper ~5 cm of each sample was cut using a rock saw at Boston University. Samples were shipped to the Cosmogenic
Nuclide Dating Group at the Lamont-Doherty Earth Observatory for further sample processing and *in situ* nuclide extraction.

3.3.1 Cosmogenic ^{3}He in pyroxene

Samples were crushed to 63-125 μm to separate pyroxene mineral grains, rinsed thoroughly with deionized (DI) water to
remove fines, then leached in a 10% phosphoric acid solution overnight to remove oxidation and other contaminants from
mineral surfaces. The samples were then density-separated in a centrifuge using sodium polytungstate heavy liquid at a
density of 3.0 g·cm^{-3}; the sinking fraction was rinsed with de-ionized water and dried overnight. Magnetic minerals were
removed using a Frantz magnetic separator set between 0.4 and 0.5 amps. The non-magnetic fraction was then leached in a
2% HNO$_3$/2% HF solution on a shaker table overnight, then rinsed, dried, and packed in aluminium foil for analysis. Helium
isotopes were measured with the LDEO MAP 215–50 noble gas mass spectrometer using an air standard. Previous
cosmogenic nuclide studies show that pyroxene from Ferrar Dolerite contains non-trivial amounts of non-cosmogenic,
nucleogenic ^{3}He, which is relevant for LGM-aged sediments (Ackert, 2000; Balter-Kennedy et al., 2020; Kaplan et al., 2017;
Margerison et al., 2005). We subtracted a non-nucleogenic ^{3}He correction of 3.3 x 10^6 atoms g^{-1} (Balter-Kennedy et al.,
2020) to all ^{3}He measurements, as this is the most up-to-date correction measurement and higher correction values (5 - 7 x
10^6 atoms g^{-1}) generate some exposure ages that produce modern exposure ages that are unreasonably young. ^{3}He in
pyroxene (^{3}He$_{pyx}$) exposure ages were calculated using Version 3 of the online exposure age calculator hosted by the
University of Washington (https://hess.ess.washington.edu/) (Balco et al., 2008) assuming density of 2.9 g·cm^{-3}, corrected
for shielding and thickness, the Antarctica-specific atmospheric model (ANT) (Stone, 2000), the global ^{3}He production rate

190 $(120 \pm 9.4 \text{ atom g}^{-1} \text{ yr}^{-1})$ (Goehring et al., 2010), and used the LSDn scaling scheme (Lifton et al., 2014). We employed the LSDn scaling scheme, which is time dependent, because the compiled dataset spans a wide timescale over the past 500 kyr. We note that exposure ages using the St or Lm scaling schemes generate slightly older exposure ages, but do not change observed patterns in the wider dataset.

3.3.2 Cosmogenic ^{10}Be in quartz

195 Samples were crushed to 500-125 μm, then froth flotation was used to separate the quartz grains. Quartz separates were purified by leaching in a HNO_3/HF acid solution, and then $^{10}Be_{qtz}$ was extracted from purified quartz, both according to standard protocols in the Cosmogenic Nuclide Dating Group and established methods (Brown et al., 1991; Kohl and Nishiizumi, 1992). ^{10}Be/^{9}Be ratios were measured at the Center for Accelerator Mass Spectrometry at Lawrence Livermore National Laboratory, and normalized to 07KNSTD3110, which has an assumed ^{10}Be/^{9}Be ratio of 2.85×10^{-12} (Nishiizumi et
200 al., 2007). $^{10}Be_{qtz}$ exposure ages were calculated using the version 3 of the online exposure age calculator hosted by the University of Washington (https://hess.ess.washington.edu/) (Balco et al., 2008) assuming a rock density of 2.7 g cm^{-3} corrected for shielding and thickness, and the LSDn scaling scheme (Lifton et al., 2014) the Antarctica-specific atmospheric model (ANT) (Stone, 2000), the global ^{10}Be production rate (4.15 atoms g^{-1} yr^{-1}) (Martin et al., 2017), and used the LSDn scaling scheme (Lifton et al., 2014) for the same reasons explained for $^3He_{pyx}$ above. Four Three procedural blanks were
205 processed with samples to correct background ^{10}Be/^{9}Be (Table 3) and applied to samples according to extraction date. Blank corrections were applied to samples according to the batch in which they were processed. Two blanks (BLK1-2016Jun03, BLK2-2016Jun03) were averaged (4.6 ± 1.7 x10^{-16}) and applied to ^{10}Be/^{9}Be measurements from samples ACX-13-18, ACX-14-26, ACX-13-56. A blank correction of 4.9 ± 1.4E-16 (BLK-2016Apr12) was applied to ^{10}Be/^{9}Be measurements from samples ACX-14-08, ACX-14-16.

210 **3.4 Compiled exposure chronology**

New and previously published cosmogenic nuclide concentrations from previous studies in the McMurdo Sound region (Anderson et al., 2017; Brook et al., 1995; Joy et al., 2017) were compiled from the ICE-D database (antarctica.ice-d.org) (Balco, 2020). Updated eExposure ages for all samples were calculated version 3 of the online exposure age calculator hosted by the University of Washington (https://hess.ess.washington.edu/) using the same atmospheric model, LSDn scaling
215 scheme, and global production rates as used for the new samples in this study the LSDn scaling scheme (Lifton et al., 2014). Only samples collected from the maximum extent of Ross Sea drift were selected from previous studies; we do not include exposure ages collected from elevation transects and used for deglacial thinning chronologies. All exposure ages of older glacial deposits, however, were included as geomorphologic mapping of these deposits is less complete. Only $^{10}Be_{qtz}$ in granite, ^{3}He in olivine ($^3He_{olv}$) in basalt, and $^3He_{pyx}$ in dolerite are considered here; too few exposure ages in other erratic
220 lithologies (such as gneiss and sandstone) and $^{26}Al_{qtz}$ exist to be compared against the larger dataset. Additionally, we

exclude previously published $^3He_{qtz}$ exposure ages due to diffusion uncertainties inherent to that specific nuclide system (Brook et al., 1995).

4. Results

4.1 Glacial geologic mapping

The Upper Discovery deposit reaches a maximum elevation of 77~~0~~5 m and decreases in elevation from east to west along Mount Discovery (Fig. 4). The limit of the Upper Discovery deposit is nearly continuous and well-defined across the northern face of Mount Discovery, and is draped onto cinder cones, volcanic vents, and intervening valleys. Windswept snow fields and alpine glaciers presently cover and cross over the glacial limit in a few locations. The elevation of the glacial limit descends to ~450 m elevation on western Mount Discovery above Koettlitz Glacier where it becomes poorly defined due to disturbance from solifluction. Between the limits of the Upper Discovery deposit and Ross Sea drift on Mount Discovery, no clear moraines or intermediate glacial limits were found. Above the Upper Discovery deposit, no erratic lithologies are present – only local volcanic rocks exist.

The Upper Discovery deposit is characterized by low-relief moraines (< 1 m height) where clasts are mostly embedded in the soil matrix. Large boulders (>1 m diameter) are ~~rare~~rare, and most clasts are ~~cobble-sized~~cobble sized. Observed erratic lithologies include Ferrar Dolerite and Granite Harbor Intrusives. Clasts are characterized by varnished surfaces, ventifaction, and cavernous weathering. Patterned ground is well developed on the surface, and, unlike Ross Sea drift, thermokarst topography and features are absent along much of the upper elevation limit. Solifluction lobes are present along the northwest face of upper Mount Discovery and have disturbed the Upper Discovery deposit limit.

4.2 Cosmogenic nuclide analyses

4.2.1 New $^3He_{pyx}$ in Ferrar Dolerite exposure ages

$^3He_{pyx}$ exposure ages of Ferrar Dolerite generally sort according to the stratigraphy of mapped glacial deposits but display wide scatter within these stratigraphic groupings (Table 1). Four of the five $^3He_{pyx}$ exposure ages of Ferrar Dolerite in Ross Sea drift on eastern Mount Discovery and Brown Peninsula range between ~~27.5~~14.3 ± 1.0 ka to ~~53.2~~36.0 ± 1.~~1~~8 ka, while the remaining exposure age from a sharp-crested moraine on Brown Peninsula was much older, ~~382~~361.6 ± 10.~~9~~7 ka. $^3He_{pyx}$ exposure ages (n=4) from the Upper Discovery deposit were old; three ages are between ~~245.7~~229.2 ± 8.~~1~~0 ka and ~~262.4~~245.9 ± 13.~~9~~6 ka; the other exposure age was even older (3~~66.0~~47.9 ± 11.~~6~~4 ka).
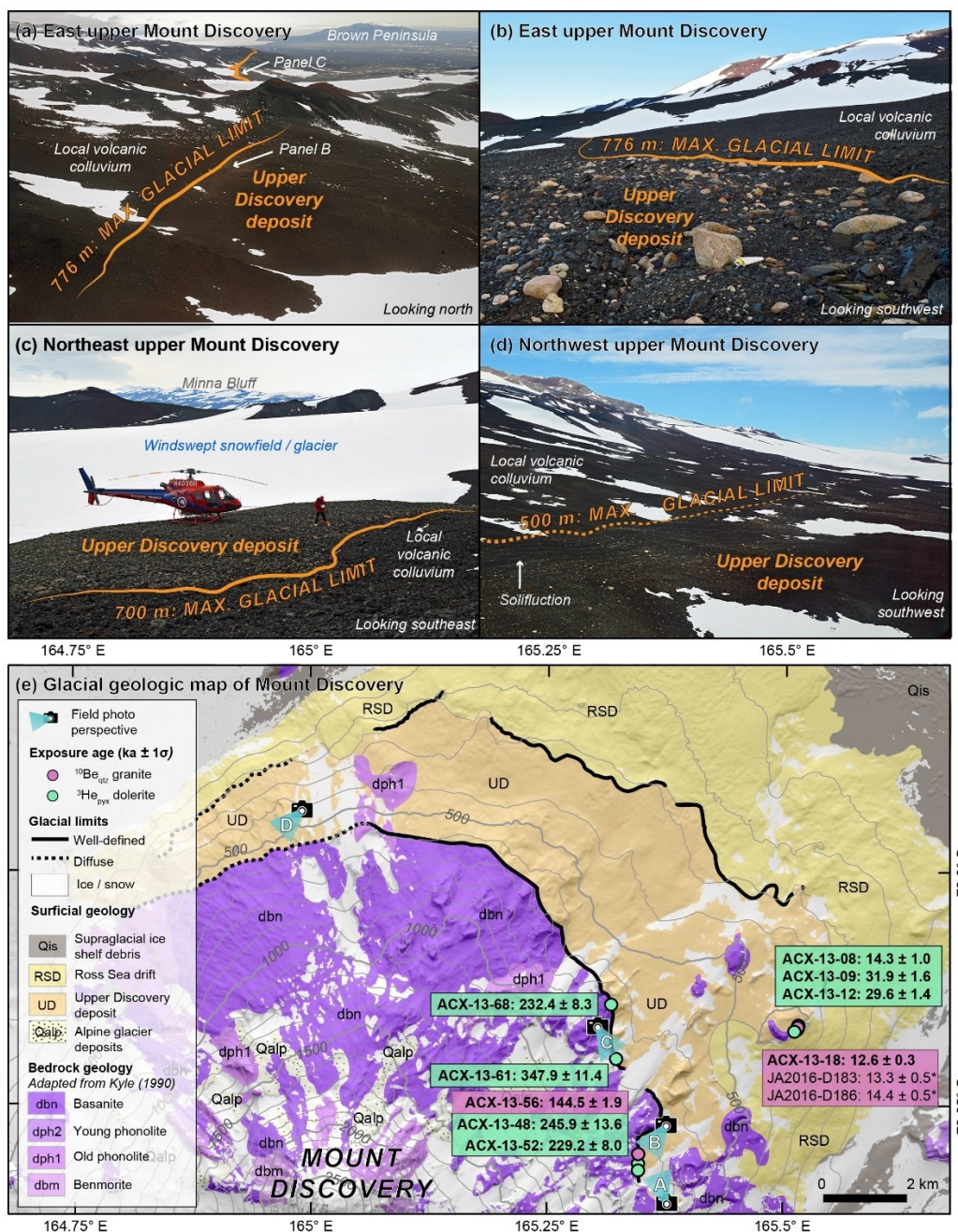
Figure 4: Upper Discovery deposit mapping and exposure ages. (a-d) Field photos show the well-defined (solid orange) and diffuse (dashed orange) glacial limits on upper Mount Discovery. (e) Glacial geologic map and cosmogenic nuclide exposure ages of glacial deposits on Mount Discovery. Camera icon shows vantage point of field photos in panels (a-d). Samples with "JA2016-" prefix are from Anderson et al., 2017; all other samples are new age constraints from this study.

Table 1: ^{3}He$_{pyroxene}$ exposure ages from Ferrar Dolerite

Sample Name	Latitude (dd)	Longitude (dd)	Elevation (m)	Location	Shielding correction	Thickness correction[a]	Measured ^{3}He concentration atoms g^{-1}	Corrected ^{3}He concentration[b] atoms g^{-1}	±1σ atoms g^{-1}	Exposure Age[c] (ka)	Internal error[c] (ka)	External error[c] (ka)
Ross Sea drift												
ACX-13-08	-78.3338	165.5146	512	Mount Discovery	0.9993	0.9770	7.04E+06	3.96E+04	2.66E+05	14.3	1.0	1.9
ACX-13-09	-78.3340	165.5140	511	Mount Discovery	0.9993	0.9778	1.16E+07	4.63E+06	4.11E+05	31.9	1.6	3.9
ACX-13-12	-78.3338	165.5146	512	Mount Discovery	0.9976	0.9757	1.10E+07	3.99E+06	3.75E+05	29.6	1.4	3.6
ACX-14-05	-78.0832	165.4644	340	Brown Peninsula	0.9810	0.9905	8.24E+07	7.54E+07	2.34E+06	361.6	10.7	41.2
ACX-14-15	-78.1002	165.3507	242	Brown Peninsula	0.9989	0.9836	1.05E+07	3.53E+06	3.61E+05	36.0	1.8	4.3
Upper Discovery deposit												
ACX-13-48	-78.3632	165.3468	775	Mount Discovery	0.9957	0.9808	8.57E+07	7.87E+07	4.55E+06	245.9	13.6	30.3
ACX-13-52	-78.3629	165.3466	774	Mount Discovery	0.9957	0.9764	7.97E+07	7.27E+07	2.65E+06	229.2	8.0	26.4
ACX-13-61	-78.3405	165.3227	702	Mount Discovery	0.9969	0.9724	1.11E+08	1.04E+08	3.53E+06	347.9	11.4	39.9
ACX-13-68	-78.3289	165.3173	707	Mount Discovery	0.9976	0.9868	7.69E+07	6.99E+07	2.62E+06	232.4	8.3	26.9

Table 1: ^{3}He$_{pyx}$ exposure age from Ferrar Dolerite. [a] ~~Assumed~~[a] Assumed density for all samples = 2.9 g/cm3. [b] Corrected for 3.3E+06 atoms/g contribution of nucleogenic 3He in Ferrar Dolerite (Balter-Kennedy et al., 2020). [c] Exposure ages were calculated using Version 3 of the online exposure age calculator hosted by the University of Washington (https://hess.ess.washington.edu/) (Balco et al., 2008) using the Antarctica-specific atmospheric model (ANT) (Stone, 2000), the global ^{3}He production rate (Goehring et al., 2010), and used the LSDn scaling scheme (Lifton et al., 2014) ~~bResults calculated using Cronus Online Calculator v3 with LSDn scaling scheme (Lifton et al., 2014).~~

4.2.2 New $^{10}Be_{qtz}$ in granite exposure ages

$^{10}Be_{qtz}$ exposure ages of granite sort according to stratigraphic age and display less scatter than $^{3}He_{pyx}$ exposure ages (Table 2). $^{10}Be_{qtz}$ exposure ages of clasts from Ross Sea drift on Mount Discovery and Brown Peninsula had two younger and
265 similar ages (12.6 ± 0.3 ka, 12.8 ± 0.3 ka); and two older ages (20.2 ± 0.6 ka, 34.2 ± 0.7 ka). A single exposure age of a cavernously weathered boulder in the Upper Discovery deposit yielded an age of 144.5 ± 1.9 ka.

Sample Name	Latitude (dd)	Longitude (dd)	Elevation (m)	Location	Quartz mass (g) [a]	LLNL Cathode #	Mass ^{9}Be added (µg) [a]	Uncorrected ^{10}Be/^{9}Be Ratio [b]	±1σ [c]	Background corrected [c,d] ^{10}Be/^{9}Be Ratio	±1σ	[^{10}Be] (atoms g^{-1})	±1σ (atoms g^{-1})	Exposure Age [e] (ka)	Internal error [e] (ka)	External error [e] (ka)
Ross Sea Drift																
ACX-13-18[d]	-78.3331	165.5153	507	Mount Discovery	10.0477	BE41642	186.8	9.17E-14	2.09E-15	9.12E-14	2.10E-15	1.13E+05	2.60E+03	12.6	0.3	0.8
ACX-14-08[e]	-78.0813	165.4635	345	Brown Peninsula	4.2853	BE40972	192.2	5.21E-14	1.38E-15	5.16E-14	1.39E-15	1.55E+05	4.15E+03	20.2	0.5	1.3
ACX-14-16[e]	-78.1007	165.3478	249	Brown Peninsula	7.2061	BE40973	191.7	1.34E-13	2.54E-15	1.33E-13	2.55E-15	2.37E+05	4.53E+03	34.2	0.7	2.1
ACX-14-26[d]	-78.0882	165.3833	228	Brown Peninsula	10.0188	BE41643	187.0	7.07E-14	1.56E-15	7.02E-14	1.57E-15	8.75E+04	1.96E+03	12.8	0.3	0.8
Upper Discovery deposit																
ACX-13-56[d]	-78.3618	165.3476	772	Mount Discovery	10.0216	BE41644	187.2	1.28E-12	1.63E-14	1.28E-12	1.63E-14	1.60E+06	2.03E+04	144.5	1.9	9.0

Table 2: ^{10}Be$_{qtz}$ exposure ages from granite erratics.

Table 2: ^{10}Be$_{qtz}$ exposure ages from granite erratics. [a] Shielding correction of 1 applied to all samples. Thickness correction of 0.9833 was applied to all samples assuming a density of 2.7 g cm^{-3} for all samples. [b] ^{9}Be was added to samples prepared at LDEO through a beryl carrier made at LDEO with a concentration of 1034.9 µg mL^{-1}. [c] Isotopic analysis was conducted at the Center for Accelerator Mass Spectrometry at LLNL ~~Laboratory~~; ratios were normalized against standard 07KNSTD3110 with an assumed ratio of 2850 x 10-15 (Nishiizumi et al., 2007). [d] A blank correction of 4.6 ± 1.7E-16 (average2016Jun03) was applied to ^{10}Be/^{9}Be measurements from samples ACX-13-18, ACX-14-26, ACX-13-56. See Table 3 for details. [e] A blank correction of 4.9 ± 1.4E-16 (BLK-2016Apr12) was applied to 10Be/9Be measurements from samples ACX-14-08, ACX-14-16. See Table 3 for details. [f] Results calculated using Cronus Online Calculator v3 with LSDn scaling scheme (Lifton et al., 2014).

BLANK	Lab ID	Mass ^{9}Be Added ug	^{10}Be/^{9}Be Ratio	±1σ	BLANK ^{10}Be (atoms/g)	±1σ (atoms/g)
BLK1-2016Jun03	BE41648	187.4	3.5E-16	2.0E-16	4.34E+03	2.46E+03
BLK2-2016Jun03	BE41649	187.4	5.8E-16	1.5E-16	7.20E+03	1.88E+03
Average-2016Jun03 [a]			*4.6E-16*	*1.7E-16*	*5.77E+03*	*2.87E+02*
BLK-2016Apr12 [b]	BE40971	213.0	4.9E-16	1.4E-16	6.96E+03	1.98E+03

TABLE 3: ^{10}Be blank correction

Table 3: Blank correction for ^{10}Be measurements. [a] A blank correction of 4.6 ± 1.7E-16 (average2016Jun03) was applied to 10Be/9Be measurements from samples ACX-13-18, ACX-14-26, ACX-13-56. [b] A blank correction of 4.9 ± 1.4E-16 (BLK-2016Apr12) was applied to 10Be/9Be measurements from samples ACX-14-08, ACX-14-16.

TABLE 4: Compiled exposure ages from McMurdo Sound

Sample name	Publication	Latitude (DD)	Longitude (DD)	Elevation (m asl)	Lithology	Nuclide (target mineral)	Exposure Age (kyr)	±1σ (kyr)
Ross Sea Drift								
JA2016-D161	Anderson et al., 2017	-78.2793	163.4934	98	granite	Be-10 (qtz)	9.9	0.4
JA2016-D183	Anderson et al., 2017	-78.3335	165.5147	526	granite	Be-10 (qtz)	13.3	0.5
JA2016-D186	Anderson et al., 2017	-78.3345	165.5111	514	granite	Be-10 (qtz)	14.4	0.5
JA2016-D139	Anderson et al., 2017	-78.1719	165.2958	307	granite	Be-10 (qtz)	19.2	0.8
KBA89-240	Brook et al., 1995	-78.1333	164.1500	253	basalt	He-3 (ol)	6.6	1.4
BAK90-138	Brook et al., 1995	-77.8667	164.4167	265	basalt	He-3 (ol)	8.0	2.4
BAK90-139-1	Brook et al., 1995	-77.8667	164.4167	265	basalt	He-3 (ol)	8.2	1.0
KBA89-295	Brook et al., 1995	-78.1667	166.4000	393	basalt	He-3 (ol)	9.2	1.1
BAK90-137-1	Brook et al., 1995	-77.8667	164.4167	265	basalt	He-3 (ol)	10.3	1.0
KBA89-241	Brook et al., 1995	-78.1333	164.1500	253	basalt	He-3 (ol)	10.7	1.2
BAK90-137-2	Brook et al., 1995	-77.8667	164.4167	265	basalt	He-3 (ol)	12.6	2.2
BAK90-136	Brook et al., 1995	-77.8667	164.4167	265	basalt	He-3 (ol)	12.9	0.8
RA92-039	Brook et al., 1995	-78.3183	163.4169	345	basalt	He-3 (ol)	17.5	1.4
BAK90-139-2	Brook et al., 1995	-77.8667	164.4167	265	basalt	He-3 (ol)	21.7	2.8
KBA-89-246-2-3	Brook et al., 1995	-78.1333	164.1500	253	basalt	He-3 (ol)	22.9	4.2
RA92-040	Brook et al., 1995	-78.3183	163.4169	345	basalt	He-3 (ol)	24.1	0.9
KBA-89-246-2-1	Brook et al., 1995	-78.1333	164.1500	253	basalt	He-3 (ol)	25.0	2.4
KBA89-247	Brook et al., 1995	-78.1333	164.1500	253	basalt	He-3 (ol)	27.0	1.0
KBA-89-246-2-2	Brook et al., 1995	-78.1333	164.1500	253	basalt	He-3 (ol)	30.5	1.6
KBA89-245	Brook et al., 1995	-78.1333	164.1500	253	basalt	He-3 (ol)	32.4	15.2
KBA89-293	Brook et al., 1995	-78.1667	166.4000	393	basalt	He-3 (ol)	38.2	3.7
KBA89-296	Brook et al., 1995	-78.1667	166.4000	393	basalt	He-3 (ol)	40.0	1.8
KBA89-140	Brook et al., 1995	-77.4833	163.6667	309	basalt	He-3 (ol)	58.0	1.9
KBA89-142	Brook et al., 1995	-77.4833	163.6667	309	basalt	He-3 (ol)	85.0	2.7
RA92-041	Brook et al., 1995	-78.3183	163.4169	345	basalt	He-3 (ol)	98.2	2.8
KBA89-292	Brook et al., 1995	-78.1667	166.4000	393	basalt	He-3 (ol)	110.3	1.5
KBA89-243	Brook et al., 1995	-78.1333	164.1500	253	basalt	He-3 (ol)	208.6	1.4
KBA89-143	Brook et al., 1995	-77.4833	163.6667	309	granite	Be-10 (qtz)	47.5	3.6
MV2-4	Joy et al., 2017	-78.1120	164.1808	40	granite	Be-10 (qtz)	9.3	0.4
MV3-2	Joy et al., 2017	-78.0990	163.9871	120	granite	Be-10 (qtz)	9.4	0.6
MV2-1	Joy et al., 2017	-78.1090	164.1308	72	granite	Be-10 (qtz)	10.0	0.5
MV2-3	Joy et al., 2017	-78.0990	164.1015	27	granite	Be-10 (qtz)	12.7	0.5
MV2-5	Joy et al., 2017	-78.1080	164.1343	75	granite	Be-10 (qtz)	45.2	1.6
ACX-13-08	This publication	-78.3338	165.5146	512	dolerite	He-3 (pyx)	14.3	1.0
ACX-13-09	This publication	-78.3340	165.5140	511	dolerite	He-3 (pyx)	31.9	1.6
ACX-13-12	This publication	-78.3338	165.5146	512	dolerite	He-3 (pyx)	29.6	1.4
ACX-13-18	This publication	-78.3331	165.5153	507	granite	Be-10 (qtz)	12.6	0.3
ACX-14-05	This publication	-78.0832	165.4644	340	dolerite	He-3 (pyx)	361.6	10.7
ACX-14-08	This publication	-78.0813	165.4635	345	granite	Be-10 (qtz)	20.2	0.5
ACX-14-15	This publication	-78.1002	165.3507	242	dolerite	He-3 (pyx)	36.0	1.8
ACX-14-16	This publication	-78.0982	165.3567	220	granite	Be-10 (qtz)	34.2	0.7
ACX-14-26	This publication	-78.0882	165.3833	228	granite	Be-10 (qtz)	12.8	0.3
Older Deposits								
BAK90-141-1	Brook et al., 1995	-77.8667	163.3833	495	basalt	He-3 (ol)	160.3	2.7
BAK90-141-2	Brook et al., 1995	-77.8667	163.3833	495	basalt	He-3 (ol)	175.7	7.6
BAK90-214	Brook et al., 1995	-78.3000	163.5500	480	basalt	He-3 (ol)	448.8	27.1
BAK90-247	Brook et al., 1995	-78.2000	163.4667	545	basalt	He-3 (ol)	258.1	16.1
BAK90-249-2	Brook et al., 1995	-78.2000	163.4667	545	basalt	He-3 (ol)	85.7	5.2
BAK90-262-1	Brook et al., 1995	-77.9833	164.3167	510	basalt	He-3 (ol)	83.1	2.2
BAK90-263	Brook et al., 1995	-77.9833	164.3167	510	basalt	He-3 (ol)	215.4	5.8
KBA89-239	Brook et al., 1995	-78.1333	164.1167	374	basalt	He-3 (ol)	131.1	1.7
Upper Discovery Deposit								
ACX-13-48	This publication	-78.3632	165.3468	775	dolerite	He-3 (pyx)	245.9	13.6
ACX-13-52	This publication	-78.3629	165.3466	774	dolerite	He-3 (pyx)	229.2	8.0
ACX-13-56	This publication	-78.3618	165.3476	772	granite	Be-10 (qtz)	144.5	1.9
ACX-13-61	This publication	-78.3405	165.3227	702	dolerite	He-3 (pyx)	347.9	11.4
ACX-13-68	This publication	-78.3289	165.3173	707	dolerite	He-3 (pyx)	232.4	8.3

285 **Table 4: Compiled exposure ages from McMurdo Sound glacial deposits.** Cosmogenic nuclide data for (Anderson et al., 2017; Brook et al., 1995; Joy et al., 2017) accessed using the ICE-D database (Balco, 2020). Exposure ages calculated with version 3 of the online exposure age calculator hosted by the University of Washington (https://hess.ess.washington.edu/) using the Antarctic atmospheric model (Stone, 2000), global production rates (Goehring et al., 2010; Martin et al., 2017), and LSDn scaling scheme (Lifton et al., 2014). Sample coordinates from (Brook et al., 1995) are approximate.

290
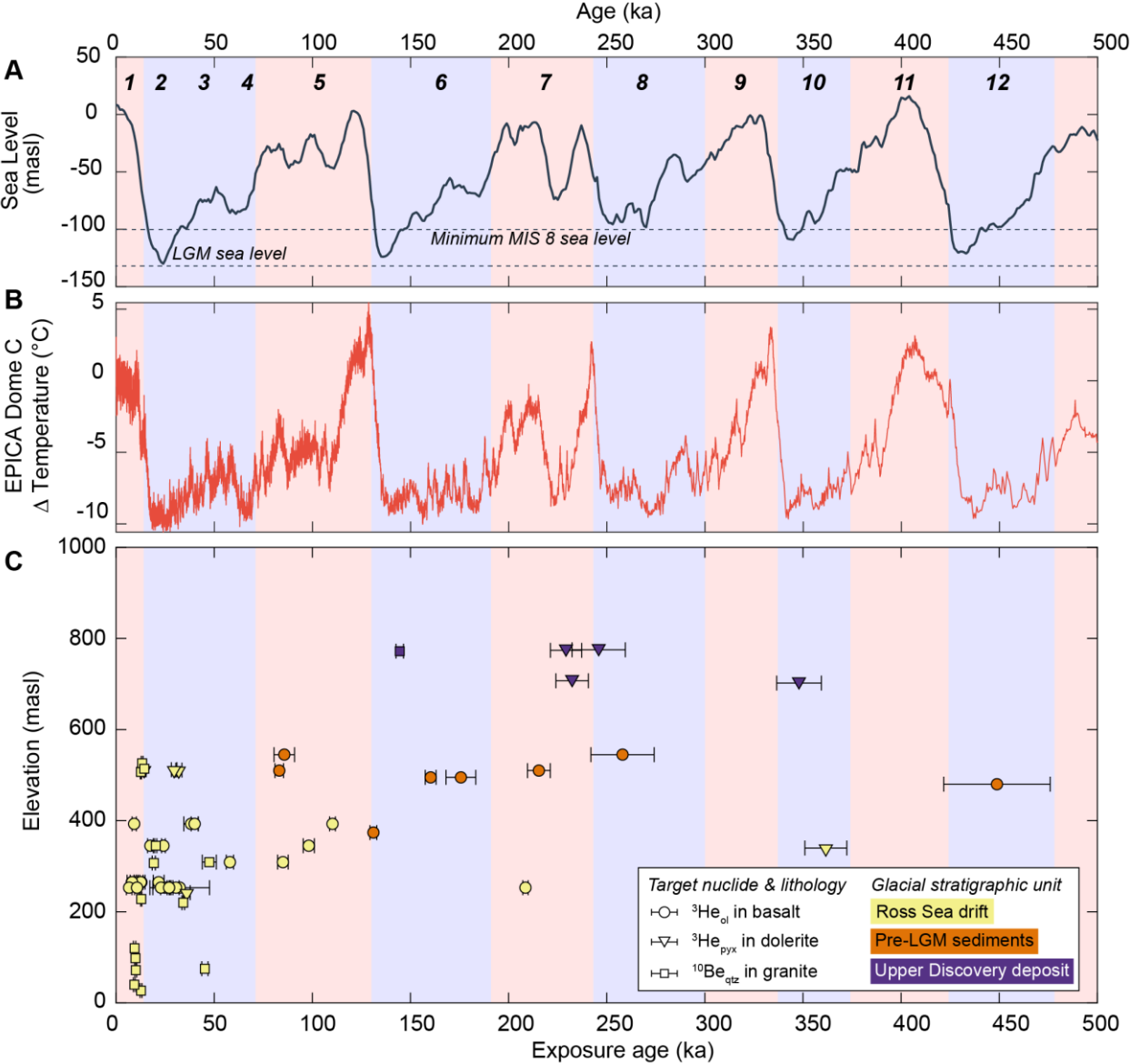
Figure 5: Exposure ages of McMurdo Sound glacial deposits in the context of paleoclimate since 500 ka. (a) Marine
Isotope Stage boundaries showing interglacial (light red) and glacial (light blue) periods, and global mean sea level (Spratt
295   and Lisiecki, 2016) - dashed blue lines show minimum global sea level during the LGM and MIS 8. (b) Temperature
difference from modern in the EPICA Dome C ice core in East Antarctica (Jouzel et al., 2007). (c) Exposure ages (±1σ error)
of Ross Sea drift (yellow circles) and older pre-LGM deposits (orange circles), ~~including the Upper Discovery deposit~~

5. Discussion

5.1 New insights from inherited nuclides and exposure age scatter

In former and active ice sheet environments, cosmogenic nuclides in glacial sediments often do not yield simple, easy-to-interpret exposure ages; instead, cosmogenic nuclides record the integrated effect of many surface processes operating on a landscape through time. Rather than focusing exclusively on the age of ice extent or retreat, cosmogenic nuclides can also be used to disentangle how glacial sediment is entrained from bedrock sources, transported by glacier ice, and deposited on the landscape. By taking advantage of the relatively simple geology of the Transantarctic Mountains, an independent (albeit rare) radiocarbon chronology, and analysis of multiple nuclides and lithologies in Ross Sea drift, we can better quantify the magnitude of and processes responsible for exposure age scatter. While scatter in exposure ages from Ross Sea drift prevents precise age constraints of maximum ice extent, it is possible to assign ages at glacial-interglacial timescales. With this information, we then consider the age of older Pleistocene glacial deposits in McMurdo Sound.

5.2 Scattered exposure ages of Ross Sea drift

The narrow range of calibrated radiocarbon ages (12.3 – 19.6 cal. ka) and scattered range of exposure ages that date to within the last glacial period confirm that Ross Sea drift is the youngest glacial deposit recording ice sheet expansion into McMurdo Sound. However, the compiled cosmogenic nuclide exposure chronology derived from multiple lithologies is highly scattered, and most individual exposure ages exceed the timeframe of local LGM ice extent established by the radiocarbon chronology. While many ages are 'too old' and suggest that these clasts carry an inventory of inherited nuclides, most of the exposure ages (with 3 exceptions) are between the early Holocene (Marine Isotope Stage [MIS] 1) and last glacial period (MIS 2 - 4). Upper elevation, weathered deposits yield much older Pleistocene ages (MIS 5 – 12) that are incompatible with a local LGM depositional age.

This exposure age dataset underscores the difficulty of using surface exposure dating in Antarctica to constrain precise ages of individual landforms or glacial deposits from the local LGM using $^{10}Be_{qtz}$, $^{3}He_{pyx}$, or $^{3}He_{olv}$. The most extreme example of scatter comes from two exposure ages from the same moraine ridge on northern Brown Peninsula. This sharp-crested moraine ridge is independently dated to 17.9 cal. ka (Christ and Bierman, 2020), but nearly adjacent clasts yield exposure ages that are both 'too old' and widely different. A perched granite cobble produced an exposure age of 20.2 ± 0.5 ka (ACX-14-08) and a nearby dolerite cobble has an exposure age of 382.8 ± 10.9 ka (ACX-14-05), the oldest of any sample from Ross Sea drift. On eastern Mount Discovery (512 m), the glacial limit is marked by a stark lithological contrast between erratic-rich Ross Sea drift lying at lower elevations than volcanic-rich glacial deposits (Anderson et al., 2017; Christ and Bierman, 2020; Denton and Marchant, 2000). Here, granite exposure ages coincide with the end of the local LGM in McMurdo Sound (12.6 to 14.4 ka, n = 3); (this study; Anderson et al., 2017), but two of the three dolerite exposure ages of

dolerite from the same location are ~~consistently~~ older (~~27.5~~ACX-13-09: 29.6 ± 1.4 ka, ACX-13-12: 31.9 ± 1.4 ka ~~to 45.5 ka, n = 3~~). Clearly, exposure ages from individual landforms from the same local LGM deposit in the McMurdo Sound region contain clasts with different exposure histories.

5.3 Surface processes contributing to exposure age scatter

335   We suggest that scatter is related to bedrock source and that specific surface processes prevent, enhance, or reduce the likelihood of nuclide inheritance prior to and during glacial entrainment and deposition. Exposure age scatter sorts according to lithology and nuclide: granite $^{10}Be_{qtz}$ exposure ages are younger, but scattered, dolerite $^{3}He_{pyx}$ ages are consistently too old, and basalt $^{3}He_{olv}$ ages slightly pre-date and post-date the local LGM. These patterns can be explained by examining how clasts were glacially entrained and incorporated into Ross Sea drift.

340 ### 5.3.1 Sub-glacial plucking reduces nuclide inheritance

Granite clasts in Ross Sea drift, sourced from Granite Harbor Intrusives, are likely entrained by sub-glacial plucking, and therefore produce younger, less-scattered exposure ages. Granite Harbor Intrusives comprise the base of the stratigraphic section for much of the Transantarctic Mountains in Southern Victoria Land (Fig. 1). The large EAIS outlet glaciers in the Transantarctic Mountains south of McMurdo Sound – Byrd Glacier, Mullock Glacier, and Skelton Glacier –

345 have all incised deep troughs that cut into Granite Harbor Intrusives (Fig. 1). Ice sheet models simulate that these outlet glaciers thicken and expand into the Ross Sea during glacial periods; they are also wet-based and erode large volumes of sediment (Golledge et al., 2013). Rock surfaces at the bottom of outlet glacier troughs are up to 1000 m below sea level and could not experience exposure to cosmic rays. In addition, the Pleistocene stability and persistence of EAIS outlet glaciers in the Transantarctic Mountains likely prevented prior exposure of the bedrock troughs (Kaplan et al., 2017). Taken together,

350 this means that Granite Harbor Intrusives plucked from the base of outlet glacier troughs are less likely to contain cosmogenic nuclides inherited from periods of exposure prior to local LGM deglaciation in Ross Sea drift. The resulting exposure ages are more likely to record clast emplacement at maximum ice extent. Ferrar Dolerite bedrock is likely present below many outlet glaciers draining the EAIS and tributary alpine glaciers in the Transantarctic Mountains. Presumably dolerite clasts are also sub-glacially plucked and entrained into over-riding ice, which would generate exposure ages that

355 reliably record clast emplacement on moraines. However, it appears that dolerite clasts in Ross Sea drift are more likely to have older than expected exposure ages that indicate a complex exposure history and nuclide inheritance.

5.3.2 Cliff exposure, rockfall, and supraglacial transport increases nuclide inheritance

Old exposure ages of several granite and nearly all dolerite clasts in Ross Sea drift may reflect prior cliff exposure and entrainment by rockfall along outlet glacier margins. Granite Harbor Intrusive rocks are exposed in cliff faces above the

360 glacier surface closer to the coast and along outlet glacier margins in the Transantarctic Mountains (Fig. 1). During previous interglacial periods or glacial low-stands when outlet glaciers were thinner (Jones et al., 2017), exposure on granite cliff

faces would have accumulated cosmogenic nuclides prior to later glacial entrainment. The effect of prior cliff exposure is likely more important for exposure ages of Ferrar Dolerite because these rocks form many of the peaks and cliff faces above glacier surfaces in the Transantarctic Mountains at elevations >1000 m (Fig. 1). Prolonged cliff exposure combined with low erosion rates (Mackay et al., 2014) at high elevations (where the cosmogenic nuclide production rate is also higher), will increase cosmogenic nuclide inventories in dolerite more than granite clasts. Additionally, $^3He_{pyx}$ is a stable cosmogenic nuclide that does not decay during burial (Dunai, 2010); this further increases the probability of nuclide inheritance in dolerite clasts. Even with the nucleogenic ^3He correction applied, dolerite $^3He_{pyx}$ exposure ages still tend to be too old, suggesting nuclide inheritance.

Despite increased outlet glacier surface elevations during glacial periods, cliff faces may not be subjected to wet-based glacial erosion due to insufficient ice thickness. Selective linear erosion below polythermal ice sheets can lead to wet-based, erosive glacial conditions in outlet glacier troughs, but cold-based, non-erosive glacial conditions along valley walls (Bentley et al., 2006; Stone et al., 2003; Sugden et al., 2005). Clasts sourced from rockfall events onto the glacier surface or reworked from older ice marginal sediments in these regions of cold-based ice will not be sufficiently eroded to remove inherited nuclides. Ferrar Dolerite may be particularly susceptible to cold-based, non-erosive glacial transport because many high-elevation cliff faces are exposed over thin alpine and valley glaciers that are tributaries to larger outlet glaciers. Dolerite clasts sourced from these areas likely carry inherited nuclides that are not removed by glacial erosion.

When rockfalls from cliff faces deliver granite or dolerite onto glacier surfaces below, inherited nuclides remain in some clasts. While rockfall onto glaciers may shatter large volumes of rock and expose fresh surfaces some clasts may retain the original surface exposed on the cliff face. Clasts that land directly onto the ice surface will accumulate additional nuclides if they remain exposed during supraglacial transport. Rockfall that does not land directly on the glacier surface, but accumulates along outlet glacier margins, could be subjected to additional exposure prior to a glacial high stand that entrains these clasts. Additionally, clasts may be repeatedly recycled by multiple glacial advance and retreat events.

5.3.3 Ice sheet reworking of local volcanic rocks causes and prevents prior exposure

$^3He_{olv}$ exposure ages of basalt clasts, sourced from the local McMurdo Volcanic Suite, record local landscape exposure prior to and following ice sheet advance (Brook et al., 1995). The bimodal distribution of $^3He_{olv}$ in basalt exposure ages predates maximum ice sheet extent in McMurdo Sound (25.0 ka) and post-dates ice thinning (9.6 ka). Clasts with inherited nuclides and excessively old exposure ages may have been initially sub-aerially exposed during a glacial low stand prior to the local LGM or the last interglacial (MIS 5). As ice advanced into McMurdo Sound during the local LGM, volcanic clasts with inherited nuclides may have been reworked into Ross Sea drift. However, clasts that lack previous exposure could be entrained from submarine sources that lack any previous exposure and transported along the base of the ice sheet in McMurdo Sound. As ice thinned and down-wasted, basal clasts would be exposed last, possibly producing exposure ages younger than the onset of ice thinning (12.3 ka), a process which could also explain some of the younger $^{10}Be_{qtz}$ exposure ages of granite in Ross Sea drift. The $^3He_{olv}$ exposure ages are compatible with ice thinning on eastern

Mount Discovery from its maximum extent after 14.0 ka to near present elevations at 7.3 ka (Anderson et al., 2017). Likewise, $^3\text{He}_{olv}$ exposure ages from the McMurdo Sound region agree with rapid lowering of outlet glaciers during the Early Holocene (Anderson et al., 2017; Goehring et al., 2019; Jones et al., 2015, 2021; Spector et al., 2017) as grounded ice in the Ross Sea retreated (Halberstadt et al., 2016; McKay et al., 2016). The $^3\text{He}_{olv}$ exposure ages are compatible with ice thinning on eastern Mount Discovery from its maximum extent after 14.0 ka to near present elevations at 7.3 ka (Anderson et al., 2017), as well as other outlet glacier thinning histories of that show rapid ice lowering during the Early Holocene (Anderson et al., 2020; Goehring et al., 2019; Jones et al., 2015, 2021; Spector et al., 2017) as grounded ice in the Ross Sea retreated (Halberstadt et al., 2016).

5.4 Upper Discovery deposit: maximum glaciation ~~during MIS 8~~of McMurdo Sound

The Upper Discovery deposit marks the maximum limit of glaciation of McMurdo Sound ~~during the end of MIS 8 (243 – 300 ka)~~. The decreasing elevation of the Upper Discovery limit around Mount Discovery from 776 m in the east to ~450 m in the west suggests a larger ice sheet in the Ross Sea overflowed into McMurdo Sound during a glacial period prior to the local LGM. As there are no erratic lithologies present above this limit, the Upper Discovery deposit delineates the largest and thickest ice sheet in the western Ross Sea to inundate McMurdo Sound since Mount Discovery formed 5.5 to 4.5 Ma (Kyle, 1990).

Taking into consideration exposure age scatter, nuclide inheritance, and the few exposure ages available in our dataset, ~~W~~it is possible~~e assign an age of late MIS 8 to~~ that the Upper Discovery deposit ~~with~~dates to glacial Termination III at the transition from the late MIS 8 glacial period to the early MIS 7 interglacial period. ~~consideration of exposure age scatter and nuclide inheritance.~~At the local LGM limit on Mount Discovery, Ross Sea drift $^3\text{He}_{pyx}$ ages exceed the $^{10}\text{Be}_{qtz}$ ages by ~~14.1 to 32.1 ka~~as much as ~15 kyr. If a similar magnitude of nuclide inheritance is assumed for the Upper Discovery deposit, three $^3\text{He}_{pyx}$ exposure ages in Ferrar Dolerite from the Upper Discovery deposit ~~still~~date within ~~MIS 8~~ early MIS 7 to late MIS 8. One older $^3\text{He}_{pyx}$ dolerite exposure age from this deposit (ACX-13-61: 3~~66.2~~47.9 ± 11.6 ka) is compatible with ~~an~~this MIS 7-8 age~~age of MIS 8~~; as observed with ~~in~~ Ross Sea drift, outlier $^3\text{He}_{pyx}$ exposure ages can be preserved in the same deposit, possibly due to clast recycling. The $^{10}\text{Be}_{qtz}$ exposure age (ACX-13-52: 153.3 ± 2.0 ka, MIS 6), is too young. However, this sample was collected above a cavernous weathering pit on a granite boulder, which clearly indicates that the boulder was eroding, and thus losing some of the inventory of ^{10}Be that accumulated since deposition; this would yield a young-biased exposure age. Even if lithology-specific boulder erosion rates for granite (13 mm kyr^{-1}) and dolerite (19 mm kyr^{-1}) (Marrero et al., 2018) in Antarctica are considered, the difference between the exposure ages of the granite boulder (147 ka) and the dolerite boulders (~226-356 ka) is too much to be explained by the difference in erosion rates between lithologies. This suggests that this particular granite boulder was weathering much faster than regional average rates or it may have been affected by post-depositional movement to generate an anomalously young age. Additional exposure age constraints from the Upper Discovery deposit as well as other higher elevation pre-LGM glacial sediments in the McMurdo Sound region will further test if a glacial high-stand occurred during MIS 8.

While our current dataset is limited by the low number of samples and exposure age scatter, Mmaximum ice sheet expansion during the end of MIS 8 is compatible with other Pleistocene glacial records in from the McMurdo Sound region.

430   Many of the exposure ages from pre-LGM glacial sediments at lower elevations in McMurdo Sound are either younger or older than those from the Upper Discovery deposit; this suggests that older Pleistocene ice sheets in McMurdo Sound were thicker than during the local LGM but were less extensive than during MIS 8. The AND-1B core in McMurdo Sound records ~5 glaciations during the last 500 ka (McKay et al., 2012). While poor core recovery in the upper part of AND-1B limits the interpretation of ice sheet behaviour during the last glaciation and interglacial, deformed till recovered from the third-to-last

435   glacial period could reflect greater ice thickness in McMurdo Sound during MIS 8 (McKay et al., 2012).

There is little evidence for a MIS 8 glacial high stand preserved in sediments along the margins of outlet glaciers that flow into McMurdo Sound during glacial periods. Clasts from the head of the Skelton Glacier drainage basin likely record multiple episodes of exposure during interglacials and burial below ice during glacial periods from the Pliocene to Pleistocene, which is compatible with increased ice thickness during MIS 8 (Jones et al., 2017). At lower elevations along

440   Skelton Glacier, most samples record ice-thinning following the LGM (Anderson et al., 2020). Due to ice cover, no cosmogenic nuclide studies from Mullock Glacier exist. Although Hatherton and Darwin glaciers transport less material into McMurdo Sound during glacial periods (Talarico et al., 2013), there is also no evidence of MIS 8 glacial sediments preserved along the margins of those glaciers (Joy et al., 2014; King et al., 2020; Storey et al., 2010). In general, exposure ages of pre-LGM glacial sediments above outlet glacier margins record glacial high-stands during MIS 6 and earlier, but

445   there is no apparent evidence for elevated outlet glaciers during MIS 8 (Anderson et al., 2020; Bromley et al., 2010; Hillenbrand et al., 2014; Joy et al., 2014; Staiger et al., 2006; Storey et al., 2010).

At a wider scale, maximum ice sheet extent in McMurdo Sound during MIS 8 may reflect the unique character of this glacial period relative to others of the past 800 kyr. During MIS 8, global ice volume was lower and average eustatic sea level was higher than the LGM (Spratt and Lisiecki, 2016); yet the marine-based ice sheet in McMurdo Sound was larger

450   than its local LGM configuration. In the EPICA Dome C ice core, the glacial termination following MIS 8 (T3) is characterized by an earlier warming between 256-249 ka that coincided with an insolation minimum in the northern hemisphere (unlike other terminations of the past 500 kyr), followed by brief cooling between 248-249 ka, and then rapid warming until 243 ka (Bréant et al., 2019). The subsequent MIS 7e interglacial, while warm in Antarctica, was globally cooler than other interglacials of the past 450 kyr (Past Interglacials Working Group of PAGES, 2016). It is possible that

455   warmer Antarctic temperatures increased accumulation, and reduced ocean forcing supported a thicker marine ice sheet in the western Ross Sea at the end of MIS 8, similar to the mechanism proposed for the persistence of grounded ice in McMurdo Sound during the last glacial termination (Hall et al., 2015).

6. Conclusion

Exposure ages of glacial deposits in the McMurdo Sound region record multiple surface processes operating in the
Transantarctic Mountains prior to, during, and following glacial entrainment throughout the Pleistocene. Ross Sea drift
contains clasts that yield exposure ages during the early Holocene and last glacial period, but generally exceed the timing of
local LGM ice extent (12.3 – 19.6 ka) established by an independent radiocarbon chronology. We attribute the scatter and
prior exposure in this dataset to surface processes related to bedrock sources for glacially eroded and transported material.
Granite clasts, sourced via sub-glacial plucking and/or rock fall, produce scattered exposure ages that are less likely to record
prior exposure. Ferrar Dolerite clasts, sourced from exposed cliff faces and high elevation peaks in the Transantarctic
Mountains above outlet glaciers, are more likely to contain inherited nuclides, due to entrainment along cold-based glacier
margins. Local volcanic rocks infrom the McMurdo Sound region produce exposure ages that record landscape exposure
prior to ice sheet advance and following ice sheet thinning, which reflects reworking of previously exposed clasts along with
clasts derived from sub-marine sources that lack any previous exposure. $^3He_{pyx}$ exposure ages of higher elevation, weathered
glacial deposits on Mount Discovery suggest that the largest Pleistocene ice sheet advanced into McMurdo Sound during the
latter halfend of MIS 8 and early MIS 7. Although the small number of samples as well as prior exposure and boulder
erosion limits a precise age of such older deposits, it may be rare geologic evidence of Antarctic ice sheet volume during
MIS 8, a glacial period marked by generally warmer Antarctic temperature and higher global sea level.

Data availability statement

All data presented in this manuscript are hosted in a repository at the Open Science Framework (Christ et al., 2021b).

Author contribution

AC designed the study, conducted field work, and analysed data, and wrote the manuscript with contributions from all co-authors. PB edited the manuscript and provided mentorship. JL, JS, and GW conducted laboratory analyses and edited the
manuscript.

Competing interests

The authors declare that they have no conflict of interest.

Acknowledgements

This project was funded by NSF Office of Polar Programs award 1246316. We appreciate the field assistance from E. Chamberlain, N. Robinson, D. Rybarcyzk, S. Mackay, D. Kowalewski, and A. Canty; laboratory assistance from R. Schwartz and J. Sparks.

References

Ackert, R. P.: Antarctic Glacial Chronology : New constraints from surface exposure dating by U- ', PhD Thesis, 2000.

Anderson, J. B.: Antarctic marine geology, New York : Cambridge University Press, New York., 1999.

Anderson, J. T. H., Wilson, G. S., Fink, D., Lilly, K., Levy, R. H. and Townsend, D.: Reconciling marine and terrestrial evidence for post LGM ice sheet retreat in southern McMurdo Sound, Antarctica, Quat. Sci. Rev., 157, 1–13, https://doi.org/10.1016/j.quascirev.2016.12.007, 2017.

Anderson, J. T. H., Wilson, G. S., Selwyn Jones, R., Fink, D. and Fujioka, T.: Ice surface lowering of Skelton Glacier, Transantarctic Mountains, since the Last Glacial Maximum: Implications for retreat of grounded ice in the western Ross Sea, , https://doi.org/10.1016/j.quascirev.2020.106305, 2020.

Arndt, J. E., Schenke, H. W., Jakobsson, M., Nitsche, F. O., Buys, G., Goleby, B., Rebesco, M., Bohoyo, F., Hong, J., Black, J., Greku, R., Udintsev, G., Barrios, F., Reynoso-Peralta, W., Taisei, M. and Wigley, R.: The international bathymetric chart of the Southern Ocean (IBCSO) version 1.0-A new bathymetric compilation covering circum-Antarctic waters, Geophys. Res. Lett., 40(12), 3111–3117, https://doi.org/10.1002/grl.50413, 2013.

Balco, G.: Technical note: A prototype transparent-middle-layer data management and analysis infrastructure for cosmogenic-nuclide exposure dating, Geochronology, 2(2), 169–175, https://doi.org/10.5194/gchron-2-169-2020, 2020.

Balco, G., Stone, J. O., Lifton, N. A. and Dunai, T. J.: A complete and easily accessible means of calculating surface exposure ages or erosion rates from 10 Be and 26 Al measurements, Quat. Geochronol., 3, 174–195, https://doi.org/10.1016/j.quageo.2007.12.001, 2008.

Balco, G., Schaefer, J. M. and Grp, L.: Exposure-age record of Holocene ice sheet and ice shelf change in the northeast Antarctic Peninsula, Quat. Sci. Rev., 59, 101–111, https://doi.org/10.1016/j.quascirev.2012.10.022, 2013.

Balco, G., Blard, P. H., Shuster, D. L., Stone, J. O. H. and Zimmermann, L.: Cosmogenic and nucleogenic 21Ne in quartz in a 28-meter sandstone core from the McMurdo Dry Valleys, Antarctica, Quat. Geochronol., 52, 63–76,

https://doi.org/10.1016/j.quageo.2019.02.006, 2019.

Balter-Kennedy, A., Bromley, G., Balco, G., Thomas, H. and Jackson, M.: A 14.5 million-year record of East Antarctic Ice
Sheet fluctuations from the central Transantarctic Mountains, constrained with cosmogenic 3He, 10Be, Ne, and 26Al, Cryosph.
Discuss., 14, 2647–2672, https://doi.org/10.5194/tc-2020-57, 2020.

Bennett, M. and Glasser, N. F.: Glacial geology : ice sheets and landforms, Wiley, Chichester ; New York., 1996.

Bentley, M. J., Fogwill, C. J., Kubik, P. W. and Sugden, D. E.: Geomorphological evidence and cosmogenic 10Be/26Al
exposure ages for the Last Glacial Maximum and deglaciation of the Antarctic Peninsula Ice Sheet, Geol. Soc. Am. Bull.,
118(9–10), 1149–1159, https://doi.org/10.1130/B25735.1, 2006.

Bentley, M. J., Cofaigh, C. O., Anderson, J. B., Conway, H., Davies, B., Graham, A. G. C., Hillenbrand, C. D., Hodgson, D.
a., Jamieson, S. S. R., Larter, R. D., Mackintosh, A., Smith, J. a., Verleyen, E., Ackert, R. P., Bart, P. J., Berg, S., Brunstein,
D., Canals, M., Colhoun, E. a., Crosta, X., Dickens, W. a., Domack, E., Dowdeswell, J. a., Dunbar, R., Ehrmann, W., Evans,
J., Favier, V., Fink, D., Fogwill, C. J., Glasser, N. F., Gohl, K., Golledge, N. R., Goodwin, I., Gore, D. B., Greenwood, S. L.,
Hall, B. L., Hall, K., Hedding, D. W., Hein, A. S., Hocking, E. P., Jakobsson, M., Johnson, J. S., Jomelli, V., Jones, R. S.,
Klages, J. P., Kristoffersen, Y., Kuhn, G., Leventer, A., Licht, K., Lilly, K., Lindow, J., Livingstone, S. J., Masse, G., McGlone,
M. S., McKay, R. M., Melles, M., Miura, H., Mulvaney, R., Nel, W., Nitsche, F. O., O'Brien, P. E., Post, A. L., Roberts, S. J.,
Saunders, K. M., Selkirk, P. M., Simms, A. R., Spiegel, C., Stolldorf, T. D., Sugden, D. E., van der Putten, N., van Ommen,
T., Verfaillie, D., Vyverman, W., Wagner, B., White, D. a., Witus, A. E., Zwartz, D., Consortium, R., Ó Cofaigh, C., Anderson,
J. B., Conway, H., Davies, B., Graham, A. G. C., Hillenbrand, C. D., Hodgson, D. a., Jamieson, S. S. R., Larter, R. D.,
Mackintosh, A., Smith, J. a., Verleyen, E., Ackert, R. P., Bart, P. J., Berg, S., Brunstein, D., Canals, M., Colhoun, E. a., Crosta,
X., Dickens, W. a., Domack, E., et al.: A community-based geological reconstruction of Antarctic Ice Sheet deglaciation since
the Last Glacial Maximum, Quat. Sci. Rev., 100, 1–9, https://doi.org/10.1016/j.quascirev.2014.06.025, 2014.

Bierman, P. R., Shakun, J. D., Corbett, L. B., Zimmerman, S. R. and Rood, D. H.: A persistent and dynamic East Greenland
Ice Sheet over the past 7.5 million years, Nature, 540(7632), 256–260, https://doi.org/10.1038/nature20147, 2016.

Bréant, C., Landais, A., Orsi, A., Martinerie, P., Extier, T., Prié, F., Stenni, B., Jouzel, J., Masson-Delmotte, V. and
Leuenberger, M.: Unveiling the anatomy of Termination 3 using water and air isotopes in the Dome C ice core, East Antarctica,
Quat. Sci. Rev., 211, 156–165, https://doi.org/10.1016/j.quascirev.2019.03.025, 2019.

Briner, J. P., Kaufman, D. S., Manley, W. F., Finkel, R. C. and Caffee, M. W.: Cosmogenic exposure dating of late Pleistocene
moraine stabilization in Alaska, Bull. Geol. Soc. Am., 117(7–8), 1108–1120, https://doi.org/10.1130/B25649.1, 2005.

Briner, J. P., Miller, G. H., Davis, P. T. and Finkel, R. C.: Cosmogenic radionuclides from fiord landscapes support differential erosion by overriding ice sheets, GSA Bull., 118(3–4), 406–420, https://doi.org/10.1130/b25716.1, 2006.

Briner, J. P., Lifton, N. A., Miller, G. H., Refsnider, K., Anderson, R. and Finkel, R.: Using in situ cosmogenic Be-10, C-14, and Al-26 to decipher the history of polythermal ice sheets on Baffin Island, Arctic Canada, Quat. Geochronol., 19, 4–13, https://doi.org/10.1016/j.quageo.2012.11.005, 2014.

Bromley, G. R. M. M., Hall, B. L., Stone, J. O., Conway, H. and Todd, C. E.: Late Cenozoic deposits at Reedy Glacier, Transantarctic Mountains: implications for former thickness of the West Antarctic Ice Sheet, Quat. Sci. Rev., 29(3–4), 384–398, https://doi.org/10.1016/j.quascirev.2009.07.001, 2010.

Brook, E. J., Kurz, M. D., Ackert, R. P., Denton, G. H., Brown, E. T., Raisbeck, G. M. and Yiou, F.: Chronology of Taylor Glacier Advances in Arena Valley, Antarctica, Using in Situ Cosmogenic 3He and 10Be, Quat. Res., 39(1), 11–23, https://doi.org/10.1006/qres.1993.1002, 1993.

Brook, E. J., Kurz, M. D., Ackert, R. P., Raisbeck, G. and Yiou, F.: Cosmogenic nuclide exposure ages and glacial history of late Quaternary Ross Sea drift in McMurdo Sound, Antarctica, Earth Planet. Sci. Lett., 131(1–2), 41–56, https://doi.org/10.1016/0012-821X(95)00006-X, 1995.

Brown, E. T., Edmond, J. M., Raisbeck, G. M., Yiou, F. F., Kurz, M. D. and Brook, E. J.: Examination of surface exposure ages of Antarctic moraines using in situ produced 10Be and 26Al, Geochim. Cosmochim. Acta, 55(8), 2269–2283, https://doi.org/10.1016/0016-7037(91)90103-C, 1991.

Christ, A. J. and Bierman, P. R.: The local last glacial maximum in McMurdo Sound, Antarctica: Implications for ice-sheet behavior in the ross sea embayment, Bull. Geol. Soc. Am., 132(1–2), 31–47, https://doi.org/10.1130/B35139.1, 2020.

Christ, A. J., Bierman, P. R., Schaefer, J. M., Dahl-Jensen, D., Steffensen, J. P., Corbett, L. B., Peteet, D., Thomas, E. K., Steig, E. J., Rittenour, T. M., Tison, J.-L., Blard, P. H., Perdial, N., Dethier, D., Lini, A., Hidy, A. J., Caffee, M. W. and Southon, J. R.: A multi-million-year-old record of Greenland vegetation and glacial history preserved in sediment beneath 1.4 km of ice at Camp Century, Proc. Natl. Acad. Sci., 118(13), e2021442118, https://doi.org/10.1073/pnas.2021442118, 2021a.

Christ, A. J., Bierman, P. R., Lamp, J. L., Schaefer, J. M. and Winckler, G.: Dataset: Cosmogenic nuclide exposure age scatter in McMurdo Sound, Antarctica records Pleistocene glacial history and processes, , https://doi.org/10.17605/OSF.IO/XH5EW, 2021b.

Cook, K. L., Whipple, K. X., Heimsath, A. M. and Hanks, T. C.: Rapid incision of the Colorado River in Glen Canyon; insights

from channel profiles, local incision rates, and modeling of lithologic controls, Earth Surf. Process. Landforms, 34(7), 994–1010, https://doi.org/10.1002/esp.1790, 2009.

565 Corbett, L. B., Bierman, P. R. and Rood, D. H.: Constraining multi-stage exposure-burial scenarios for boulders preserved beneath cold-based glacial ice in Thule, northwest Greenland, Earth Planet. Sci. Lett., 440(C), 147–157, https://doi.org/10.1016/j.epsl.2016.02.004, 2016.

Corbett, L. B., Bierman, P. R., Wright, S. F., Shakun, J. D., Davis, P. T., Goehring, B. M., Halsted, C. T., Koester, A. J., Caffee, M. W. and Zimmerman, S. R.: Analysis of multiple cosmogenic nuclides constrains Laurentide Ice Sheet history and
570 process on Mt. Mansfield, Vermont's highest peak, Quat. Sci. Rev., 205, 234–246, https://doi.org/10.1016/j.quascirev.2018.12.014, 2019.

Davis, P. T., Bierman, P. R., Marsella, K. A., Caffee, M. W. and Southon, J. R.: Cosmogenic analysis of glacial terrains in the eastern Canadian Arctic: A test for inherited nuclides and the effectiveness of glacial erosion, Ann. Glaciol., 28, 181–188, https://doi.org/10.3189/172756499781821805, 1999.

575 Denton, G. H. and Marchant, D. R.: The geologic basis for a reconstruction of a grounded ice sheet in McMurdo Sound, Antarctica, at the Last Glacial Maximum, Geogr. Ann. Ser. A, Phys. Geogr., 2000.

Dunai, T. J.: Cosmogenic Nuclides: Principles, Concepts and Applications in the Earth Surface Sciences, Cambridge University Press, Cambridge., 2010.

Fitzgerald, P.: Tectonics and landscape evolution of the Antarctic plate since the breakup of Gondwana, with an emphasis on
580 the West Antarctic Rift System and the Transantarctic Mountains, R. Soc. New Zeal. Bull., 35, 453–469, 2002.

Goehring, B. M., Kurz, M. D., Balco, G., Schaefer, J. M., Licciardi, J. and Lifton, N.: A reevaluation of in situ cosmogenic 3He production rates, Quat. Geochronol., 5(4), 410–418, https://doi.org/https://doi.org/10.1016/j.quageo.2010.03.001, 2010.

Goehring, B. M., Balco, G., Todd, C., Moening-Swanson, I. and Nichols, K.: Late-glacial grounding line retreat in the northern Ross Sea, Antarctica, Geology, 47(4), 291–294, https://doi.org/10.1130/G45413.1, 2019.

585 Golledge, N. R., Levy, R. H., McKay, R. M., Fogwill, C. J., White, D. A., Graham, A. G. C., Smith, J. A., Hillenbrand, C. D., Licht, K. J., Denton, G. H., Ackert, R. P., Maas, S. M. and Hall, B. L.: Glaciology and geological signature of the Last Glacial Maximum Antarctic ice sheet, Quat. Sci. Rev., 78, 225–247, https://doi.org/10.1016/j.quascirev.2013.08.011, 2013.

Greenwood, S. L., Simkins, L. M., Halberstadt, A. R. W., Prothro, L. O. and Anderson, J. B.: Holocene reconfiguration and readvance of the East Antarctic Ice Sheet, Nat. Commun., 9(1), 3176, https://doi.org/10.1038/s41467-018-05625-3, 2018.

590 Grindley, G. W. and Laird, M. G.: Geologic Map of Antarctica Sheet 15, Shackleton Coast, 1969.

Halberstadt, A. R. W., Simkins, L. M., Greenwood, S. L. and Anderson, J. B.: Past ice-sheet behaviour: retreat scenarios and changing controls in the Ross Sea, Antarctica, Cryosphere, 10(3), 1003–1020, https://doi.org/10.5194/tc-10-1003-2016, 2016.

Hall, B. L. and Denton, G. H.: Radiocarbon chronology of Ross Sea drift, eastern Taylor Valley, Antarctica; evidence for a grounded ice sheet in the Ross Sea at the last glacial maximum, Geogr. Ann. Ser. A Phys. Geogr., 82(2–3), 305–336, 595 https://doi.org/10.1111/j.0435-3676.2000.00127.x, 2000.

Hall, B. L., Denton, G. H., Heath, S. L., Jackson, M. S. and Koffman, T. N. B.: Accumulation and marine forcing of ice dynamics in the western Ross Sea during the last deglaciation, Nat. Geosci., 8(8), 1–28, https://doi.org/10.1038/ngeo2478, 2015.

Hein, A. S., Fogwill, C. J., Sugden, D. E. and Xu, S.: Geological scatter of cosmogenic-nuclide exposure ages in the Shackleton 600 Range,   Antarctica: Implications   for   glacial   history,   Quat.   Geochronol.,   19,   52–66, https://doi.org/10.1016/j.quageo.2013.03.008, 2014.

Heyman, J., Stroeven, A. P., Harbor, J. M., M.W., C. and Caffee, M. W.: Too young or too old: Evaluating cosmogenic exposure dating based on an analysis of compiled boulder exposure ages, Earth Planet. Sci. Lett., 302(1), 71–80, https://doi.org/https://doi.org/10.1016/j.epsl.2010.11.040, 2011.

605 Hillenbrand, C. D., Bentley, M. J., Stolldorf, T. D., Hein, A. S., Kuhn, G., Graham, A. G. C., Fogwill, C. J., Kristoffersen, Y., Smith, J. a., Anderson, J. B., Larter, R. D., Melles, M., Hodgson, D. a., Mulvaney, R. and Sugden, D. E.: Reconstruction of changes in the Weddell Sea sector of the Antarctic Ice Sheet since the Last Glacial Maximum, Quat. Sci. Rev., 100, 111–136, https://doi.org/10.1016/j.quascirev.2013.07.020, 2014.

Howat, I. M., Porter, C., Smith, B. E., Noh, M. J. and Morin, P.: The Reference Elevation Model of Antarctica, Cryosph., 13, 610 665–674, https://doi.org/10.5194/tc-13-665-2019, 2019.

Jackson, M. S., Hall, B. L. and Denton, G. H.: Asynchronous behavior of the Antarctic Ice Sheet and local glaciers during and since   Termination   1,   Salmon   Valley,   Antarctica,   Earth   Planet.   Sci.   Lett.,   482,   396–406, https://doi.org/10.1016/j.epsl.2017.11.038, 2018.

Jamieson, S. S. R., Sugden, D. E. and Hulton, N. R. J.: The evolution of the subglacial landscape of Antarctica, Earth Planet. 615 Sci. Lett., 293(1–2), 1–27, https://doi.org/10.1016/j.epsl.2010.02.012, 2010.

Jones, R. S., Mackintosh, A. N., Norton, K. P., Golledge, N. R., Fogwill, C. J., Kubik, P. W., Christl, M. and Greenwood, S.

L.: Rapid Holocene thinning of an East Antarctic outlet glacier driven by marine ice sheet instability, Nat. Commun., 6, 8910, https://doi.org/10.1038/ncomms9910, 2015.

Jones, R. S., K.P., N., Mackintosh, A. N., Anderson, J. T. H., Kubik, P., Vockenhuber, C., Wittmann, H., Fink, D., Wilson, G. S., Golledge, N. R. and McKay, R.: Cosmogenic nuclides constrain surface fluctuations of an East Antarctic outlet glacier since the Pliocene, Earth Planet. Sci. Lett., 480, 75–86, https://doi.org/https://doi.org/10.1016/j.epsl.2017.09.014, 2017.

Jones, R. S., Whitmore, R. J., Mackintosh, A. N., Norton, K. P., Eaves, S. R., Stutz, J. and Christl, M.: Regional-Scale abrupt Mid-Holocene Ice sheet thinning in the Western Ross Sea, Antarctica, Geology, 49(3), 278–282, https://doi.org/10.1130/G48347.1, 2021.

Jouzel, J., Masson-Delmotte, V., Cattani, O., Dreyfus, G., Falourd, S., Hoffmann, G., Minster, B., Nouet, J., Barnola, J. M., Chappellaz, J., Fischer, H., Gallet, J. C., Johnsen, S., Leuenberger, M., Loulergue, L., Luethi, D., Oerter, H., Parrenin, F., Raisbeck, G., Raynaud, D., Schilt, A., Schwander, J., Selmo, E., Souchez, R., Spahni, R., Stauffer, B., Steffensen, J. P., Stenni, B., Stocker, T. F., Tison, J. L., Werner, M. and Wolff, E. W.: Orbital and millennial antarctic climate variability over the past 800,000 years, Science (80-.)., 317(5839), 793–796, https://doi.org/10.1126/science.1141038, 2007.

Joy, K., Fink, D., Storey, B. and Atkins, C.: A 2 million year glacial chronology of the Hatherton Glacier, Antarctica and implications for the size of the East Antarctic Ice Sheet at the Last Glacial Maximum, Quat. Sci. Rev., 83, 46–57, https://doi.org/10.1016/j.quascirev.2013.10.028, 2014.

Joy, K., Fink, D., Storey, B., De Pascale, G. P., Quigley, M. and Fujioka, T.: Cosmogenic evidence for limited local LGM glacial expansion, Denton Hills, Antarctica, Quat. Sci. Rev., 178, 89–101, https://doi.org/10.1016/j.quascirev.2017.11.002, 2017.

Kaplan, M. R., Licht, K. J., Winckler, G., Schaefer, J. M., Bader, N., Mathieson, C., Roberts, M., Kassab, C. M., Schwartz, R. and Graly, J. A.: Middle to Late Pleistocene stability of the central East Antarctic Ice Sheet at the head of Law Glacier, Geology, 45(11), 963–966, https://doi.org/10.1130/g39189.1, 2017.

King, C., Hall, B., Hillebrand, T. and Stone, J.: Delayed maximum and recession of an East Antarctic outlet glacier, Geology, 48(6), 630–634, https://doi.org/10.1130/G47297.1, 2020.

Koester, A. J., Shakun, J. D., Bierman, P. R., Davis, P. T., Corbett, L. B., Goehring, B. M., Vickers, A. and Zimmerman, S. R.: Laurentide Ice Sheet thinning and erosive regimes at Mount Washington, New Hampshire, inferred from multiple cosmogenic nuclides, GSA Spec. Pap., 2020.

Kohl, C. P. and Nishiizumi, K.: Chemical isolation of quartz for measurement of in-situ -produced cosmogenic nuclides, Geochim. Cosmochim. Acta, 56(9), 3583–3587, https://doi.org/10.1016/0016-7037(92)90401-4, 1992.

Lamp, J. L., Marchant, D. R., Mackay, S. L. and Head, J. W.: Thermal stress weathering and the spalling of Antarctic rocks, J. Geophys. Res. Earth Surf., 122(1), 3–24, https://doi.org/10.1002/2016JF003992, 2017.

Lewis, A. and Ashworth, A.: An early to middle Miocene record of ice-sheet and landscape evolution from the Friis Hills, Antarctica, Geol. Soc. Am. Bull., 128(5–6), 719–738, https://doi.org/10.1130/B31319.1, 2016.

Lewis, A. R., Marchant, D. R., Ashworth, A. C., Hedenas, L., Hemming, S. R., Johnson, J. V, Leng, M. J., Machlus, M. L., Newton, A. E., Raine, J. I., Willenbring, J. K., Williams, M. and Wolfe, A. P.: Mid-Miocene cooling and the extinction of tundra in continental Antarctica, Proc. Natl. Acad. Sci., 105(31), 10676–10680, https://doi.org/10.1073/pnas.0802501105, 2008.

Lifton, N., Sato, T. and Dunai, T. J.: Scaling in situ cosmogenic nuclide production rates using analytical approximations to atmospheric cosmic-ray fluxes, Earth Planet. Sci. Lett., 386, 149–160, https://doi.org/10.1016/j.epsl.2013.10.052, 2014.

Mackay, S. L., Marchant, D. R., Lamp, J. L. and Head, J. W.: Cold-based debris-covered glaciers: Evaluating their potential as climate archives through studies of ground-penetrating radar and surface morphology, J. Geophys. Res. Earth Surf., 119(11), 2505–2540, https://doi.org/10.1002/2014jf003178, 2014.

Margerison, H. R., Phillips, W. M., Stuart, F. M. and Sugden, D. E.: Cosmogenic 3He concentrations in ancient flood deposits from the Coombs Hills, northern Dry Valleys, East Antarctica: interpreting exposure ages and erosion rates, Earth Planet. Sci. Lett., 230(1–2), 163–175, https://doi.org/10.1016/j.epsl.2004.11.007, 2005.

Marrero, S. M., Hein, A. S., Naylor, M., Attal, M., Shanks, R., Winter, K., Woodward, J., Dunning, S., Westoby, M. and Sugden, D.: Controls on subaerial erosion rates in Antarctica, Earth Planet. Sci. Lett., 501, 56–66, https://doi.org/10.1016/j.epsl.2018.08.018, 2018.

Martin, L. C. P., Blard, P. H., Balco, G., Lavé, J., Delunel, R., Lifton, N. and Laurent, V.: The CREp program and the ICE-D production rate calibration database: A fully parameterizable and updated online tool to compute cosmic-ray exposure ages, Quat. Geochronol., 38, 25–49, https://doi.org/10.1016/j.quageo.2016.11.006, 2017.

McKay, R., Naish, T., Powell, R., Barrett, P., Scherer, R., Talarico, F., Kyle, P., Monien, D., Kuhn, G., Jackolski, C. and Williams, T.: Pleistocene variability of Antarctic Ice Sheet extent in the Ross Embayment, Quat. Sci. Rev., 34, 93–112, https://doi.org/10.1016/j.quascirev.2011.12.012, 2012.

McKay, R., Golledge, N. R., Maas, S., Naish, T., Levy, R., Dunbar, G. and Kuhn, G.: Antarctic marine ice-sheet retreat in the Ross Sea during the early Holocene, Geology, 44(1), 7–10, https://doi.org/10.1130/G37315.1, 2016.

Nichols, K. A., Goehring, B. M., Balco, G., Johnson, J. S., Hein, A. S. and Todd, C.: New Last Glacial Maximum ice thickness constraints for the Weddell Sea Embayment, Antarctica, Cryosphere, 13(11), 2935–2951, https://doi.org/10.5194/tc-13-2935-2019, 2019.

Nishiizumi, K., Imamura, M., Caffee, M. W., Southon, J. R., Finkel, R. C. and McAninch, J.: Absolute calibration of 10Be AMS standards, Nucl. Instruments Methods Phys. Res. Sect. B Beam Interact. with Mater. Atoms, 258(2), 403–413, https://doi.org/https://doi.org/10.1016/j.nimb.2007.01.297, 2007.

Owen, L. A., Frankel, K. L., Knott, J. R., Reynhout, S., Finkel, R. C., Dolan, J. F. and Lee, J.: Beryllium-10 terrestrial cosmogenic nuclide surface exposure dating of Quaternary landforms in Death Valley, Geomorphology, 125(4), 541–557, https://doi.org/10.1016/j.geomorph.2010.10.024, 2011.

Past Interglacials Working Group of PAGES: Interglacials of the last 800,000 years, Rev. Geophys., 54(1), 162–219, https://doi.org/doi:10.1002/2015RG000482, 2016.

Portenga, E. W., Bierman, P. R., Trodick, C. D., Greene, S. E., DeJong, B. D., Rood, D. H. and Pavich, M. J.: Erosion rates and sediment flux within the Potomac River basin quantified over millennial timescales using beryllium isotopes, Bull. Geol. Soc. Am., 131(7–8), 1295–1311, https://doi.org/10.1130/B31840.1, 2019.

Schaefer, J. M., Finkel, R. C., Balco, G., Alley, R. B., Caffee, M. W., Briner, J. P., Young, N. E., Gow, A. J. and Schwartz, R.: Greenland was nearly ice-free for extended periods during the Pleistocene, Nature, 540(7632), 252–255, https://doi.org/10.1038/nature20146, 2016.

Shakun, J. D., Corbett, L. B., Bierman, P. R., Underwood, K., Rizzo, D. M., Susan, R., Zimmerman, S. R., Caffee, M. W., Naish, T., Golledge, N. R., Hay, C. C. and Susan, R.: Minimal East Antarctic Ice Sheet retreat onto land during the past eight million years, Nature, 558(7709), 284–287, https://doi.org/10.1038/s41586-018-0155-6, 2018.

Spector, P., Stone, J., Cowdery, S. G., Conway, H., Bromley, G., Hall, B., Conway, H. and Bromley, G.: Rapid early-Holocene deglaciation in the Ross Sea , Antarctica, Geophys. Res. Lett., 44(15), 7817–7825, https://doi.org/10.1002/2017GL074216, 2017.

Spratt, R. M. and Lisiecki, L. E.: A Late Pleistocene sea level stack, Clim. Past, 12(4), 1079–1092, https://doi.org/10.5194/cp-12-1079-2016, 2016.

Staiger, J. W., Marchant, D. R., Schaefer, J. M., Oberholzer, P., Johnson, J. V., Lewis, A. R. and Swanger, K. M.: Plio-Pleistocene history of Ferrar Glacier, Antarctica: Implications for climate and ice sheet stability, Earth Planet. Sci. Lett., 243(3–4), 489–503, https://doi.org/10.1016/j.epsl.2006.01.037, 2006.

Stone, J. O.: Air pressure and cosmogenic isotope production, J. Geophys. Res., 105(B10), 23753–23759, 2000.

Stone, J. O., Balco, G. A., Sugden, D. E., Caffee, M. W., Sass, L. C., Cowdery, S. G. and Siddoway, C.: Holocene deglaciation of Marie Byrd Land, West Antarctica., Science, 299(5603), 99–102, https://doi.org/10.1126/science.1077998, 2003.

Storey, B. C., Fink, D., Hood, D., Joy, K., Shulmeister, J., Riger-Kusk, M. and Stevens, M. I.: Cosmogenic nuclide exposure age constraints on the glacial history of the Lake Wellman area, Darwin Mountains, Antarctica, Antarct. Sci., 22(06), 603–618, https://doi.org/10.1017/S0954102010000799, 2010.

Stuiver, M., Denton, G. H., Hughes, T. J. and Fastook, J. L.: History of the marine ice sheet in West Antarctica during the last glaciation: A working hypothesis, in The Last Great Ice Sheets, edited by G. H. Denton and T. J. Hughes, John Wiley and Sons, New York, , 1981.

Sugden, D. and Denton, G.: Cenozoic landscape evolution of the Convoy Range to Mackay Glacier area, Transantarctic Mountains: Onshore to offshore synthesis, Geol. Soc. Am. Bull., 116(7), 840, https://doi.org/10.1130/B25356.1, 2004.

Sugden, D. E., Balco, G., Cowdery, S. G., Stone, J. O. and Sass, L. C.: Selective glacial erosion and weathering zones in the coastal mountains of Marie Byrd Land, Antarctica, Geomorphology, 67(3–4), 317–334, https://doi.org/10.1016/j.geomorph.2004.10.007, 2005.

Sugden, D. E., Bentley, M. J. and O Cofaigh, C.: Geological and geomorphological insights into Antarctic ice sheet evolution., Philos. Trans. A. Math. Phys. Eng. Sci., 364(1844), 1607–25, https://doi.org/10.1098/rsta.2006.1791, 2006.

Sugden, D. E., Fogwill, C. J., Hein, A. S., Stuart, F. M., Kerr, A. R. and Kubik, P. W.: Emergence of the Shackleton Range from beneath the Antarctic Ice Sheet due to glacial erosion, Geomorphology, 208, 190–199, https://doi.org/10.1016/j.geomorph.2013.12.004, 2014.

Swanger, K. M., Marchant, D. R., Schaefer, J. M., Winckler, G., Head, J. W. and Head, J. W.: Elevated East Antarctic outlet glaciers during warmer-than-present climates in southern Victoria Land, Glob. Planet. Change, 79(1–2), 61–72, https://doi.org/10.1016/j.gloplacha.2011.07.012, 2011.

Talarico, F. M., McKay, R. M., Powell, R. D., Sandroni, S. and Naish, T.: Late Cenozoic oscillations of Antarctic ice sheets revealed by provenance of basement clasts and grain detrital modes in ANDRILL core AND-1B, Glob. Planet. Change, 96–

725   97, 23–40, https://doi.org/10.1016/j.gloplacha.2009.12.002, 2012.

Talarico, F. M., Pace, D. and Levy, R. H.: Provenance of basement erratics in Quaternary coastal moraines, southern McMurdo Sound, and implications for the source of Eocene sedimentary rocks, Antarct. Sci., 25(05), 681–695, https://doi.org/10.1017/S0954102013000072, 2013.

Trenhaile, A. S.: Shore platform erosion and evolution: Implications for cosmogenic nuclide analysis, Mar. Geol., 403, 80–92,
730   https://doi.org/10.1016/j.margeo.2018.05.005, 2018.

Warren, G.: Geologic Map of Antarctica Sheet 14, Terra Nova Bay to McMurdo Sound Area, 1969.

Wells, S. G., McFadden, L. D., Poths, J. and Olinger, C. T.: Cosmogenic 3He surface-exposure dating of stone pavements: Implications for landscape evolution in deserts, Geology, 23(7), 613–616, https://doi.org/10.1130/0091-7613(1995)023<0613:chsedo>2.3.co;2, 1995.

735   Young, N., Briner, J. P., Maurer, J. and Schaefer, J.: Be-10 measurements in bedrock constrain erosion beneath the Greenland Ice Sheet margin, Geophys. Res. Lett., 43(22), 11708–11719, https://doi.org/10.1002/2016GL071267, 2016.